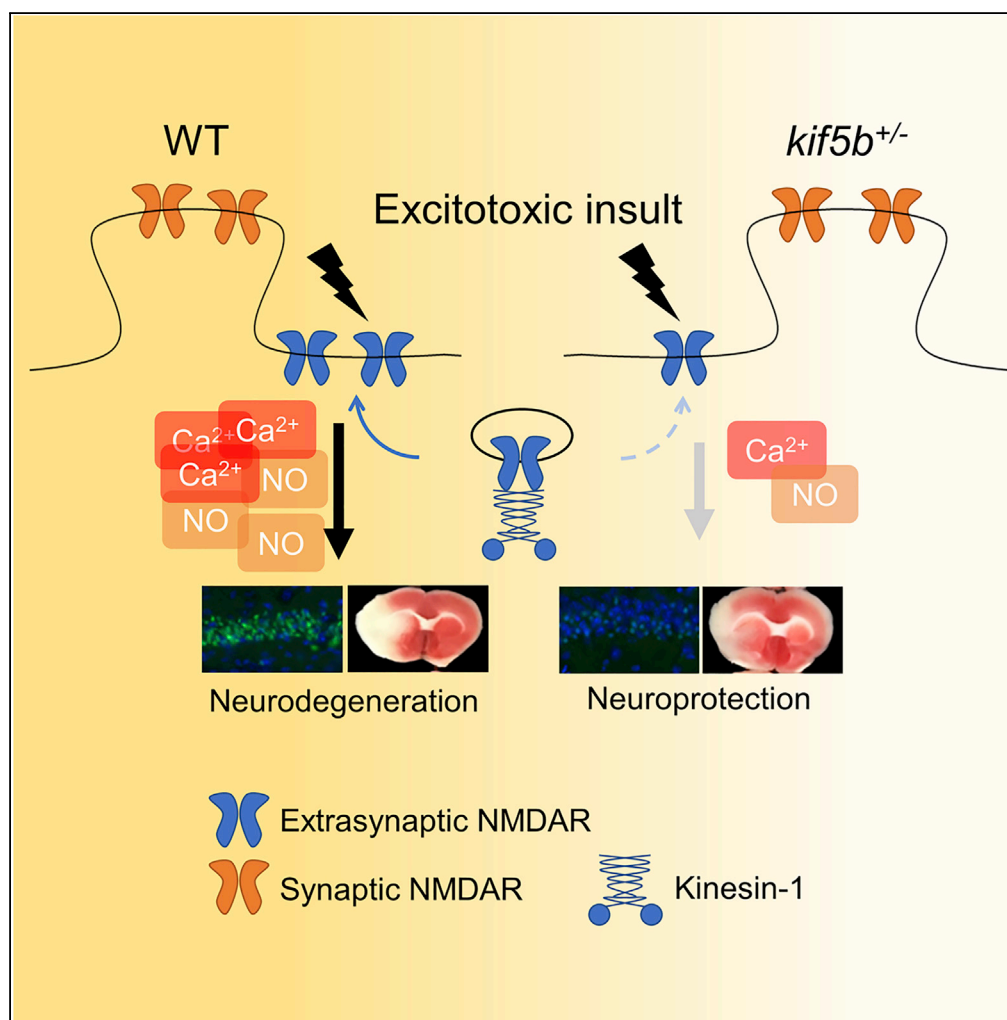**Article**

Kinesin-1 Regulates Extrasynaptic Targeting of NMDARs and Neuronal Vulnerability Toward Excitotoxicity

Raozhou Lin, Zhigang Duan, Haitao Sun, ..., Jun Xia, Jiangang Shen, Jian-Dong Huang

jdhuang@hku.hk

HIGHLIGHTS

Kif5b directly binds with GluN2B-containing NMDAR

Kinesin-1 mediates extrasynaptic NMDAR targeting and function

Reduction of kinesin-1 protects neurons against NMDAR-elicited excitotoxicity

Reduction of kinesin-1 protects brain against ischemia-elicited neurodegeneration

Article

Kinesin-1 Regulates Extrasynaptic Targeting of NMDARs and Neuronal Vulnerability Toward Excitotoxicity

Raozhou Lin,[1,14] Zhigang Duan,[1,14] Haitao Sun,[1,2,8,14] Man-Lung Fung,[1,14] Hansen Chen,[3] Jing Wang,[1] Chi-Fai Lau,[1] Di Yang,[4] Yu Liu,[1] Yanxiang Ni,[1,5] Zai Wang,[6] Ju Cui,[7] Wutian Wu,[1,9] Wing-Ho Yung,[10] Ying-Shing Chan,[1,2] Amy C.Y. Lo,[4] Jun Xia,[11] Jiangang Shen,[3] and Jian-Dong Huang[1,2,12,13,15,]*

SUMMARY

N-methyl-D-aspartate (NMDA) receptor (NMDAR) is highly compartmentalized in neurons, and its dysfunction has been implicated in various neuropsychiatric and neurodegenerative disorders. Recent failure to exploit NMDAR antagonization as a potential therapeutic target has driven the need to identify molecular mechanisms that regulate NMDAR compartmentalization. Here, we report that the reduction of Kif5b, the heavy chain of kinesin-1, protected neurons against NMDA-induced excitotoxicity and ischemia-provoked neurodegeneration. Direct binding of kinesin-1 to the GluN2B cytoplasmic tails regulated the levels of NMDAR at extrasynaptic sites and the subsequent influx of calcium mediated by extrasynaptic NMDAR by regulating the insertion of NMDARs into neuronal surface. Transient increase of Kif5b restored the surface levels of NMDAR and the decreased neuronal susceptibility to NMDA-induced excitotoxicity. The expression of Kif5b was repressed in cerebral ischemia preconditioning. Our findings reveal that kinesin-1 regulates extrasynaptic NMDAR targeting and signaling, and the reduction of kinesin-1 could be exploited to defer neurodegeneration.

INTRODUCTION

The prevalence of neuropsychiatric and neurodegenerative disorders is increasing and is putting increasing pressure on health systems. Despite the differences in the pathologies among various disorders, evidences suggest that N-methyl-D-aspartic acid (NMDA) receptor (NMDAR) dysfunction is one of the common causes (Paoletti et al., 2013; Zhou and Sheng, 2013). NMDARs belong to a group of glutamate-gated ion channels that are essential for mediating brain plasticity (Paoletti et al., 2013). These receptors have been known for decades to receive input from presynaptic neurons and convey these signals into different patterns of neuronal activity, which eventually lead to long-term changes that underlie higher cognitive functions (Paoletti et al., 2013). Pathophysiologically, the overactivation of NMDARs activates subsequent pro-death pathways such as calcium influx and the production of reactive oxygen species, which are the main causes of synaptic dysfunction and neuronal death underlying neurodegenerative disorders, like stroke and Alzheimer disease. Despite huge clinical potential, current attempts to translate NMDAR blockade into clinical applications have so far been unsatisfactory. The concern raised in inhibiting NMDARs might result from the complexity of NMDAR compartmentalization.

There are two distinct pools of NMDARs. Compared with the well-established role of the synaptic NMDARs in mediating synaptic plasticity (Paoletti et al., 2013; Thomas and Huganir, 2004), the understanding on the extrasynaptic NMDARs is elusive. It has been reported that extrasynaptic NMDAR is activated by excessively released and spillover glutamate, and consequently shuts off the pro-survival pathway elicited by synaptic NMDARs (Bading, 2013; Hardingham et al., 2002). The extrasynaptic NMDAR-induced excitotoxicity has been implicated in various neurodegenerative conditions, including stroke and Alzheimer disease (Bading, 2017; Molokanova et al., 2014; Okamoto et al., 2009; Sattler et al., 1999; Tu et al., 2010). As such, direct and overall inhibition of NMDARs might disrupt NMDAR signaling in all compartments, including the physiological NMDAR signaling that benefits the neurons (Bading, 2017; De Keyser et al., 1999; Sanacora et al., 2017). It is therefore urged to understand the mechanism that regulates the compartmentalization of NMDARs, which can be exploited to abate pathophysiological NMDAR signaling with minimal adverse physiological impacts.

[1]School of Biomedical Sciences, Li Ka Shing Faculty of Medicine, The University of Hong Kong, Pokfulam, Hong Kong

[2]State Key Laboratory of Brain and Cognitive Sciences, Li Ka Shing Faculty of Medicine, The University of Hong Kong, Pokfulam, Hong Kong

[3]School of Chinese Medicine, Li Ka Shing Faculty of Medicine, The University of Hong Kong, Pokfulam, Hong Kong

[4]Department of Ophthalmology, Li Ka Shing Faculty of Medicine, The University of Hong Kong, Pokfulam, Hong Kong

[5]Key Laboratory of Optoelectronic Devices and Systems of Ministry of Education and Guangdong Province, College of Optoelectronic Engineering, Shenzhen University, Shenzhen, China

[6]Institute of Clinical Medical Sciences, China-Japan Friendship Hospital, Beijing, China

[7]Beijing Institute of Geriatrics, Beijing Hospital, Ministry of Health, Beijing, China

[8]Department of Neurosurgery, Zhujiang Hospital, Southern Medical University, Guangzhou, China

[9]GHM Institute of CNS Regeneration, Jinan University, Guangzhou, China

[10]School of Biomedical Sciences, The Chinese University of Hong Kong, Shatin, Hong Kong

[11]Division of Life Sciences, The Hong Kong University of

Owing to their highly polarized structure, neurons rely heavily on intracellular transportation systems to maintain the highly compartmentalized signaling that integrates and processes information from different inputs and sub-neuronal compartments (Hirokawa et al., 2010; Terenzio et al., 2017). Kinesin-1 is a molecular motor complex consisting of two heavy and two light chains. One of the heavy chains, Kif5b, is composed of three functional domains: the head domain drives anterograde transport along microtubules powered by ATP hydrolysis, the stalk domain facilitates the dimerization of heavy chains, and the tail domain mediates cargo binding (Hirokawa et al., 2010; Verhey et al., 2011). Kinesin-1 with intact Kif5b is critical for development, as demonstrated by homozygous knockout of *kif5b* in mice, which causes embryonic death as early as 9.5 days *in utero* (Tanaka et al., 1998). Moreover, kinesin-1 dysfunction is implicated in the pathogenesis of various neurodegenerative disorders. For example, Kif5b-containing vast vesicles, an early hallmark of axonal transport defect, are found in the post-mortem brain of patients with Alzheimer's disease (Stokin et al., 2005), and reduced levels of kinesin heavy chains are found in the early stages of Parkinson disease, which precedes alteration of dopaminergic markers (Chu et al., 2012).

Here we identified kinesin-1 as a microtubule-dependent molecular motor that regulates the distribution and function of extrasynaptic NMDARs. Kinesin-1 binds with GluN2B NMDARs via their carboxyl tails. The reduction of kinesin-1 prevents extrasynaptic NMDAR targeting, inhibits calcium influx from extrasynaptic NMDARs, and protects neuron against NMDA-elicited excitotoxicity and ischemia-evoked neurodegeneration. Furthermore, the expression of kinesin genes, including *kif5b*, is reduced in the transcriptome of cerebral ischemia preconditioning, indicating the reduction of kinesin-1 as an intrinsic neuroprotective mechanism by regulation of the compartmentalization of signaling.

RESULTS

Kif5b Binds with GluN2B-Containing NMDARs

To test the hypothesis that kinesin-1 regulates the compartmentalization of NMDARs, we first immunoprecipitated endogenous kinesin-1 from mouse brain lysate using antibodies against Kif5b and detected GluN1, GluN2A, and GluN2B NMDAR subunits in the precipitate (Figure 1A). Reciprocal immunoprecipitation using an antibody against GluN1 further confirmed the presence of this complex (Figure S1A). Moreover, Kif5b and GluN2B were found to share partial co-localization in both soma and dendrites as seen in labeled primary hippocampal neurons at 14 days *in vitro* (DIV) using corresponding antibodies (Figure 1B). These data revealed that kinesin-1 and NMDAR form complex *in vivo*.

The Kif5b protein consists of the head domain that acts as the motor for moving along the microtubule, the coiled-coil stalk domain that forms a motor complex with other heavy chains, and the tail domain that binds to cargo. Two functional sites within the tail domain have been identified, a microtubule sliding site and an autoinhibitory site (Kaan et al., 2011; Wong and Rice, 2010). We generated a series of Kif5b truncations conjugated with a glutathione S-transferase (GST) tag in a pull-down experiment to investigate this interaction in detail (Figure 1C). We found that the Kif5b tail (850–915 amino acid [aa]) including the microtubule sliding site, which was outside the KLC-binding domain, mediated binding to NMDAR (Figures S1B and S1C). This mapping result was confirmed by the co-expression of FLAG-tagged Kif5b fragments and the intermediate tail (1,040–1,261 aa) of GluN2B in a 293T cell line and co-immunoprecipitation by FLAG (Figure 1D). It is worth noting that deletion of the microtubule sliding domain (892–915 aa, ΔMs), but not the autoinhibitiory domain (918–926 aa, ΔAi), largely abolished these interactions, suggesting that this domain was important in mediating Kif5b binding with NMDARs (Figure 1D). By examining this interaction in further detail, we identified four positively charged amino acids that are conserved across species within this region (Figure 1C) and wondered whether these positively charged amino acids are required for binding with NMDAR. Mutations of either of the two positively charged amino acids (907–909 aa, RSK to SSS or AAA; 913–915 aa, RRG to SSS or AAA) abolished this binding, whereas mutations of other amino acids (910–912 aa, NMA to SSS or AAA) did not cause any disruption (Figure 1E). Furthermore, these were direct interactions, because GST-tagged Kif5b tail fragments were able to bind with *in vitro* transcribed and translated GluN2B intermediate tails (1,040–1,261 aa) in a cell-free system (Figure 1F).

To further examine the specificity of Kif5b interaction with GluN2B, we overexpressed green fluorescent protein (GFP)-tagged GluN2A/GluN1 and GluN2B/GluN1 separately in 293T cells where there is no endogenous GluN2A or GluN2B and found that Kif5b C-terminal fragment (850–963 aa) pulled down substantial amount of GluN2B/GluN1, but not GluN2A/GluN1, indicating that Kif5b might preferably bind with GluN2B over GluN2A (Figure S1D). We mapped that GluN2B (1,040–1,261 aa) sufficed binding with

Science and Technology, Clear Water Bay, Hong Kong

[12]HKU-Shenzhen Institute of Research and Innovation, Shenzhen, China

[13]Shenzhen Institute of Advanced Technologies, Shenzhen, China

[14]These authors contributed equally

[15]Lead Contact

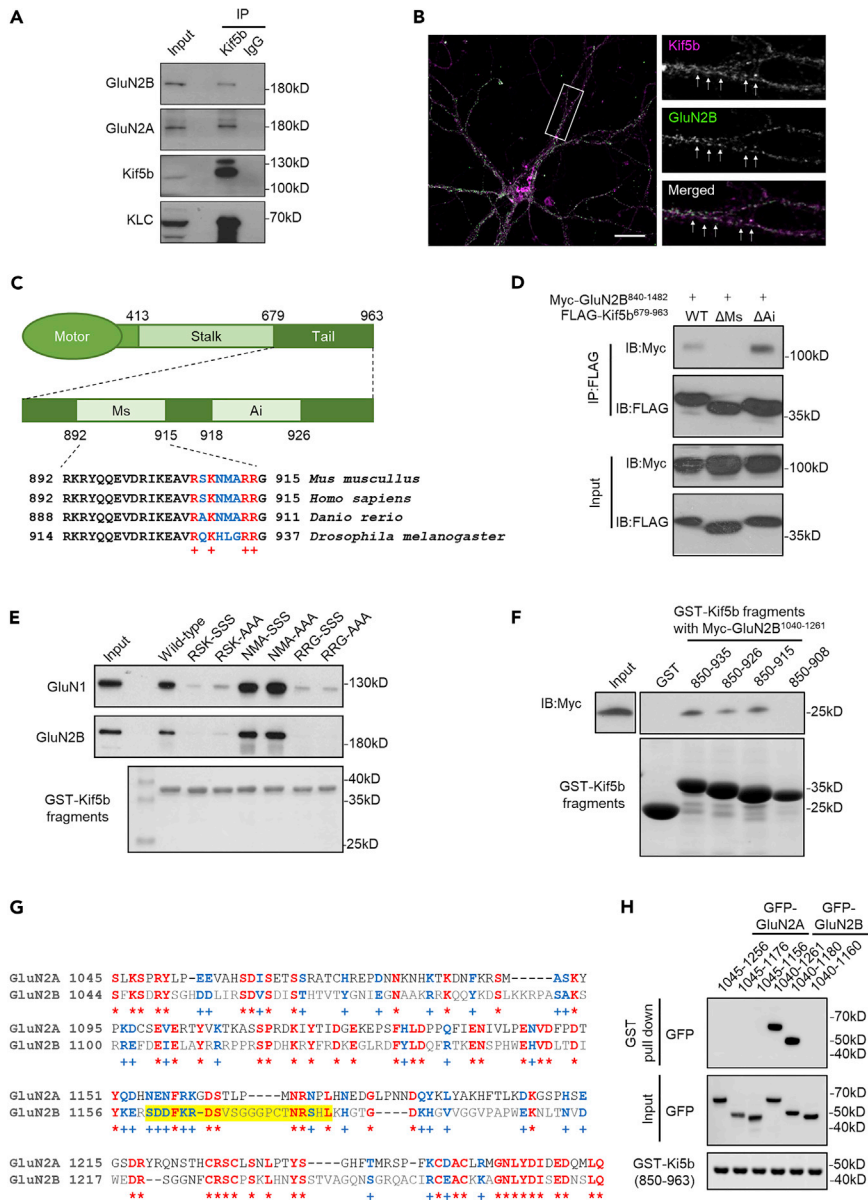*Correspondence: jdhuang@hku.hk

Figure 1. Kif5b Directly Binds with GluN2B

(A) Representative western blot images of Kif5b or normal IgG immunoprecipitation from mouse brain lysate.

(B) Immunostaining of Kif5b and GluN2B in primary hippocampal neurons (14 DIV). Scale bar (white solid line), 10 μm. The arrows in the "merged" panel indicate the co-localization signals.

(C) Schematic figure of Kif5b fragment containing the motor domain (1–413 aa), the stalk domain (414–679 aa), the tail domain (679–963 aa), the microtubule sliding domain (892–915 aa), and the autoinhibitory domain (918–926 aa). The microtubule sliding domain is conserved from *Drosophila melanogaster* to *Homo sapiens*. The four positively charged amino acids are shown in red.

(D) Representative western blot image of Kif5b tail immunoprecipitated with GluN2B intermediate tail (1,040–1,261 aa) from 293T cells overexpressing the indicated constructs.

(E) Representative western blot images of GST-tagged Kif5b tail fragment (900–935 aa) and its mutants with pull down of GluN1 and GluN2B from mouse brain lysate.

(F) Representative western blot image of GST-tagged Kif5b tail directly binding with *in vitro* transcribed and translated GluN2B intermediate tails.

(G) Sequence homology between GluN2A (1,045–1,255 aa) and GluN2B (1,044–1,261 aa). Red asterisk indicates the identical amino acid between GluN2A and GluN2B. Blue plus indicates amino acide with the same charge. Yellow highlight indicates the GluN2B tail region required for binding with Kif5b.

(H) Representative western blot image of GST-Kif5b tail (850–963 aa) binding with GluN2A and GluN2B tail fragments, as indicated.
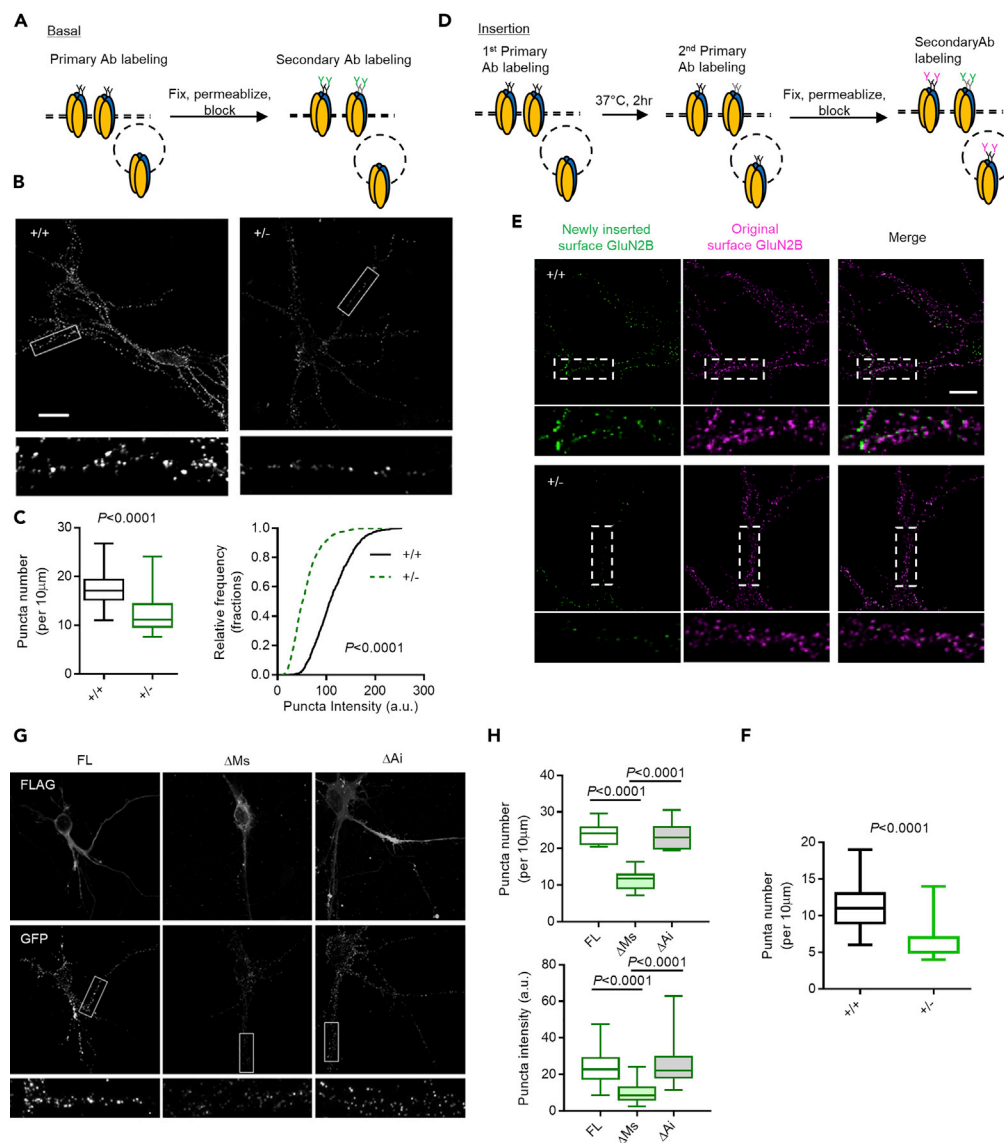
Figure 2. Kinesin-1 Regulates NMDAR Surface Expression

(A) Schematic figure showing antibody labeling the surface-GluN2B-containing NMDARs. Plasmid with extracellular GFP-tagged GluN2B was transfected into primary neuronal cultures at 14 DIV. After 24 h, neurons were incubated with anti-GFP antibody at 4°C for 1 h, followed by fixation and secondary antibody incubation.

(B and C) (B) Representative images and (C) quantification of surface GFP-GluN2B staining in primary neuronal cultures from *kif5b*^{+/−} mice (+/−) and their wild-type littermates (+/+). (C, left) Box plots show the number of puncta per 10 μm, (C, right) the curve plots show the relative intensity of each puncta (puncta number: n = 41 for wild-type and n = 39 for *kif5b*^{+/−}, five neurons were analyzed per genotype, Mann-Whitney U test; puncta intensity: six neurons were analyzed per genotype, at least 100 puncta were analyzed per neuron from three individual cultures, Kolmogorov-Smirnov test). Scale bar (white solid line), 20 μm.

(D) Schematic figure showing antibody labeling for the newly inserted GluN2B-containing NMDARs. After transfection, the neurons were saturated with chicken anti-GFP antibody for 10 min at room temperature and washed before returning to 37°C for additional 2 h. Then neurons were incubated with rabbit anti-GFP antibody for another 10 min at room temperature to label the newly inserted GluN2B. The neurons were washed, fixed, and permeabilized for secondary antibody labeling to distinguish between the newly inserted and the original GluN2B.

(E and F) (E) Representative images and (F) quantification of surface GFP-GluN2B staining in primary neuronal cultures from *kif5b*^{+/−} mice (+/−) and their wild-type littermates (+/+). (F) Box plot showed the number of puncta of newly inserted GluN2B (green channel) per 10 μm. (n = 15 per genotype; at least three neurons per genotype; for each neuron, at least three neurites were analyzed; Mann-Whitley U test). Scale bar (white solid line), 10 μm.

Figure 2. *Continued*

(G and H) (G) Representative images show surface staining of GFP-GluN2B puncta from neurons co-transfected with the indicated Kif5b constructs. Bar plots show (H, top) the average density of surface puncta and (H, bottom) the intensity of each puncta (H, top: n = 14 for FL, n = 13 for ΔMs, n = 19 for ΔAi, eight neurons analyzed for each group; H, bottom: n = 167 for FL, n = 128 for ΔMs, n = 137 for ΔAi, Kruskal-Wallis test followed by Dunn's *post hoc* test, 20 puncta/neuron analyzed for each group; three replicate experiments). Scale bar (white solid line), 20 μm. Values are presented as mean ± SEM, unless otherwise indicated (test as indicated; exact p value given if less than 0.05).

Kif5b (Figure 1F) and therefore compared the C terminal of GluN2B (1,040–1,261 aa) with that of GluN2A. GluN2A (1,045–1,255 aa) shared some similarity with GluN2B (1,044–1,261 aa, Figure 1G), but this similarity was not sufficient for the GluN2A fragment (1,046–1,255 aa) to bind with Kif5b C terminal (850–963 aa, Figure 1H). To further validate this finding, we did a series of C-terminal truncations on GluN2B and identified that GluN2B 1,160–1,180 aa was required for binding with Kif5b, as revealed that Kif5b C-terminal fragment pulled down GluN2B fragment 1,040–1,180 aa, but not 1,040–1,160 aa (Figure 1H). The above data combined reveal a complex consisting of kinesin-1 and GluN2B-containing NMDARs, indicating a role of kinesin-1 in mediating the function of GluN2B NMDARs.

Kinesin-1 Regulates Extrasynaptic NMDAR Distribution and Function

Kinesin-1 regulates transportation of cargo along microtubules through direct binding to cargo or through various adaptor proteins. This motor-cargo interaction determines the subcellular distribution of cargo and thus regulates their functions (Hirokawa et al., 2010). It has been previously reported that GluN2B-containing NMDAR is conveyed by Kif17 (Setou et al., 2000; Yin et al., 2011). Interestingly, depletion of *kif17* did not completely abolish the movement of GluN2B *in vivo* (Yin et al., 2011), raising the possibility that multiple transport systems might contribute to regulate GluN2B-containing NMDAR trafficking. To examine the functional impact of kinesin-1 on GluN2B *in vivo*, we utilized a mouse model with heterozygous knockout of *kif5b* genes, as the homozygous knockout of *kif5b* causes embryonic lethality (Tanaka et al., 1998). As expected, besides the reduced levels of Kif5b, none of the other tested kinesins was found altered, including Kif5a, Kif5c, Kif17, and Kif3 (Kif5b, p = 0.0013, t = 4.4294, df = 10; Kif5a, p = 0.5934, t = 0.5535, df = 9; Kif5c, p = 0.2031, t = 1.3619, df = 10; Kif17, p = 0.6209, t = 0.5103, df = 10; Kif3, p > 0.9999, t = 0, df = 10; unpaired t test; Figure S2A). *Kif5b$^{+/-}$* hippocampus displayed reduced levels of the kinesin-1-GluN2B complex as revealed by immunoprecipitation of Kif5b (p = 0.0005, t = 5.603, df = 8; unpaired t test; Figure S2B). Because the level of Kif17 was not altered in our *kif5b$^{+/-}$* mice (Kif17, p = 0.6209, t = 0.5103, df = 10; unpaired t test; Figure S2A), it appears that kinesin-1 reduction does not simultaneously affect Kif17-mediated transport. As such, we hypothesized that Kif5b might serve as a motor necessary for GluN2B-containing NMDAR trafficking. The western blot analysis showed no differences in the overall levels of NMDAR subunits GluN1, GluN2A, and GluN2B in hippocampal lysate in wild-type and *kif5b$^{+/-}$* mice (GluN1, p = 0.5405, t = 0.6362, df = 9; GluN2A, p = 0.4666, t = 0.7602, df = 9; GluN2B, p = 0.3506, t = 0.9845, df = 9; unpaired t test; Figure S2C). However, surface biotinylation of hippocampal slices from *kif5b$^{+/-}$* mice showed significantly reduced levels of surface GluN2B-containing NMDARs (GluN1, p = 0.0005, t = 4.672, df = 12; GluN2A, p = 0.5826, t = 0.5727, df = 8; GluN2B, p < 0.0001, t = 6.647, df = 12; unpaired t test; Figure S2D). This was further confirmed by surface labeling of primary neurons transfected with GFP-tagged GluN2B, which showed both surface GFP puncta density and intensity were reduced in *kif5b$^{+/-}$* neurons at 14–16 DIV (Figures 2A–2C; C, left, density, p < 0.0001, D = 0.6448; right, intensity, p < 0.0001, D = 0.5961; Kolmogorov-Smirnov test). To test whether kinesin-1 affects dynamic turnover of GluN2B-containing NMDAR, we performed a surface antibody labeling assay on neuronal culture from *kif5b$^{+/-}$* mice and their control littermates. We first saturated the GFP-GluN2B transfected neurons with anti-GFP antibody raised in chicken. After thorough wash, the neurons were returned to 37°C for additional 2 h to allow GluN2B turnover. The neurons were further incubated with anti-GFP antibody raised in rabbit to distinguish the original surface GluN2B from the newly inserted GluN2B (Figure 2D). Compared with the control littermates, there was a significantly reduced amount of newly inserted GluN2B in the *kif5b$^{+/-}$* cultures (p < 0.0001, U = 22.5, Mann-Whitney U test; Figures 2E and 2F).

We further examined the effect of the identified domain on mediating the GluN2B-containing NMDAR distribution. The 3×FLAG-tagged full-length Kif5b, Kif5b with microtubule sliding site deletion, or Kif5b with autoinhibitory site deletion together with GFP-GluN2B were transfected into primary cultures from *kif5b$^{+/-}$* mice. Compared with neurons expressing Kif5b with microtubule sliding site deletion, both wild-type Kif5b and Kif5b with autoinhibitory site deletion showed increased levels of both GluN2B surface puncta density and puncta intensity (density, H = 27.96, p < 0.0001; FL versus ΔMs, p < 0.0001; FL versus ΔAi, p = 0.4242;

ΔMs versus ΔAi, p < 0.0001; intensity, H = 217.0, p < 0.0001; FL versus ΔMs, p < 0.0001; FL versus ΔAi, p = 0.3565; ΔMs versus ΔAi, p < 0.0001; Kruskal-Wallis test followed by *post hoc* Dunn's multiple comparisons test; Figures 2G and 2H).

NMDAR acts as a calcium channel upon activation. The resulting calcium influx regulates synaptic strength (Bading, 2013; Volk et al., 2015) or causes the pro-death signaling cascade leading to neuronal death when it is overloaded (Bading, 2013; Tu et al., 2010). NMDAR-dependent calcium influx is associated with synaptic dysfunction and neuronal loss in both acute and chronic neurodegenerative conditions (Bading, 2013; Zhou and Sheng, 2013). To gain insight on the functional impact of kinesin-1 on NMDAR compartmentalization, we used Fluo-3 to quantify calcium influx. In $kif5b^{+/-}$ neurons, we found that NMDA-induced calcium influx was significantly reduced (Genotype, $F(1, 12,000) = 17,333$, p < 0.0001; two-way ANOVA followed by Sidak *post hoc* test; peak, p < 0.0001, U = 68.00; Mann-Whitney U test; Figure S3A), possibly indicating NMDAR hypofunction or a more generalized defect in calcium homeostasis. To distinguish between these two possibilities, we depolarized the neurons with KCl (70 mM), which triggered a similar level of calcium influx in both genotypes (Genotype, $F(1, 4,240) = 19.63$, p < 0.0001; two-way ANOVA followed by Sidak *post hoc* test; peak, p = 0.1561, U = 289.0; Mann-Whitney U test; Figure S3B). This result reassured that the reduced calcium influx in $kif5b^{+/-}$ was caused by NMDAR hypofunction.

On the neuron surface, NMDARs are distributed in postsynaptic densities (PSDs) as well as in extrasynaptic regions, and the compartmentalization determines their signaling and functions. Given the notion that GluN2B is predominately concentrated in the extrasynaptic regions in the adult mouse hippocampus (Tovar and Westbrook, 1999), we hypothesized that the kinesin-1-NMDAR complex would in a biased manner regulate the targeting and functioning of extrasynaptic NMDARs. To test this hypothesis, we immunostained surface GFP-GluN2B together with the PSD marker, PSD-95, to distinguish different NMDAR compartments at the same dendrite. Similar numbers of synaptic puncta containing GluN2B and PSD-95 were found in both wild-type and $kif5b^{+/-}$ groups (p = 0.3767, t = 1.266, df = 58; two-way ANOVA followed by Sidak *post hoc* test), whereas we observed a significant reduction of surface GFP-GluN2B signals that were not co-localized with PSD-95 in $kif5b^{+/-}$ neurons (p < 0.0001, t = 9.280, df = 58; two-way ANOVA followed by Sidak *post hoc* test; Figures 3A and 3B). These data showed that the surface targeting of extrasynaptic NMDARs was dampened by reducing kinesin-1 level. To examine the functional impact of kinesin-1 on extrasynaptic NMDAR, we monitored the calcium influx elicited by bicuculline, which increases neuronal activity by blocking a GABA A receptor, together with 4-aminopyridine (4-AP), a non-competitive NMDAR antagonist. We observed a calcium influx that was believed to be synapse specific. We then added MK-801, which targets NMDAR calcium channel opening, to block only the activated NMDAR (Hardingham et al., 2002). We did not detect any notable differences in calcium influx between the wild-type and $kif5b^{+/-}$ neurons, suggesting that synaptic NMDAR-dependent calcium influx was not altered in $kif5b^{+/-}$ neurons (p = 0.8232, U = 325.0; Mann-Whitney U test; Figures 3C and 3D). As MK-801 is demonstrated to irreversibly block extrasynaptic NMDAR, we re-stimulated the neurons after MK-801 blockade with NMDA to examine extrasynaptic NMDAR-dependent calcium influx, which showed a significant reduction in $kif5b^{+/-}$ neurons (p < 0.0001, U = 14.0; Mann-Whitney U test; Figures 3C and 3D). Taken together, the above data showed that kinesin-1 binding with GluN2B mediates NMDAR compartmentalization by regulating the extrasynaptic targeting of NMDARs, and thereby regulates NMDA-elicited calcium influx. This further indicates a role of kinesin in determining cargo destination toward different neuronal sub-compartments.

Kinesin-1 Reduction Attenuated NMDA-Elicited Excitotoxicity and Ischemia-Induced Neurodegeneration

Nitric oxide (NO) is one of the main downstream molecules generated from NMDAR overactivation and acts as one of the main mediators for NMDAR-induced excitotoxicity (Sattler et al., 1999). It is generated preferably from extrasynaptic NMDARs under certain neurodegenerative conditions (Molokanova et al., 2014). We used an NO-sensitive electrode to measure NO emissions from acutely prepared hippocampal slices from wild-type and $Kif5b^{+/-}$ mice (Tjong et al., 2007). Hypoxia (N_2) and L-arginine (L-Arg) induced significantly lower NO emissions in $kif5b^{+/-}$ slices than in wild-type (L-Arg, p < 0.0001, t = 9.53, df = 9; N_2, p < 0.0001, t = 15.53, df = 8; unpaired t test; Figure S4A). Activation of NMDARs by NMDA (50 μM) or L-glutamate (L-Glu; 4 μM) together with glycine (Gly; 20 μM) increased NO emissions in both genotypes, but the amount was significantly less in $kif5b^{+/-}$ slices (L-Glu, p < 0.0001, t = 27.10, df = 17; NMDA, p < 0.0001, t = 29.26 df = 6; unpaired t test; Figures S4B and S4C). The NO emissions from both genotypes were greatly suppressed by NMDAR blocker MK-801 (100 μM) and NO synthase (NOS) inhibitor
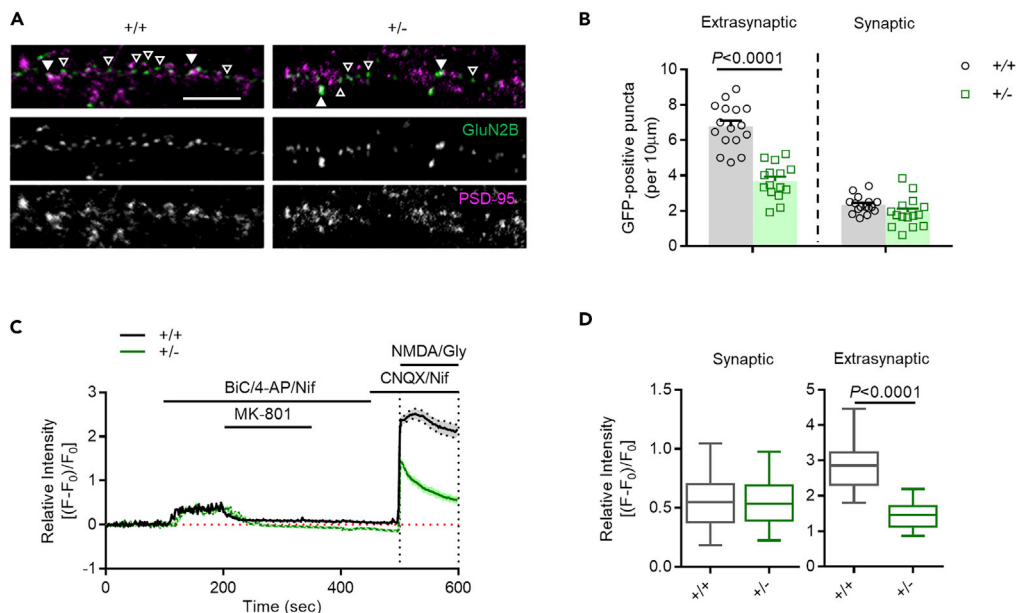
Figure 3. Kinesin-1 Regulates Extrasynaptic NMDAR Surface Targeting and Function

(A and B) (A) Representative images and (B) quantification of surface GFP-GluN2B co-localized with PSD-95 (n = 16 for wild-type and n = 15 for *kif5b*$^{+/-}$, unpaired t test; six images per genotype; scale bar, 10 μm).

(C and D) (C) Time lapse and (D) peak response (box plot) of calcium influx by synaptic and extrasynaptic NMDAR stimulation of *kif5b*$^{+/-}$ (+/−) and wild-type (+/+) neurons. *Kif5b*$^{+/-}$ (+/−) and wild-type (+/+) neurons evoked by bicuculline (Bic; 20 μM)/4-AP (4 mM) in the presence of nifedipine (Nif; 10 μM) and then blocked by MK-801 (10 μM), an irreversible NMDA receptor calcium channel blocker. The difference before and after MK-801 blockage was elicited by synaptic NMDARs. After 100 s of resting, NMDA and glycine were applied to activate the extrasynaptic NMDARs. The relative intensity $[(F-F_0)/F_0]$ was calculated (n = 27 for wild-type and n = 25 for *kif5b*$^{+/-}$ from two replicate experiments; D, Mann-Whitney U test; scale bar, 20 μm). Values are presented as mean ± SEM, unless otherwise indicated (test as indicated; exact p value given if less than 0.05).

NG-Monomethyl-L-arginine (L-NMMA; 100 μM), indicating the NO emission was NMDAR and NOS dependent (Genotype × treatment, p < 0.0001, F(2,19) = 162.8; L-Glu versus L-Glu/L-NMMA, p < 0.0001, t = 28.97, df = 19; L-Glu versus L-Glu/MK-801, p < 0.0001, t = 30.68, df = 19; two-way ANOVA followed by Sidak *post hoc* test; Figure S4D). Furthermore, in slices with NMDARs blocked by MK-801 (10 μM), depolarization using KCl (50 mM) produced similar levels of NO emissions in both genotypes (KCl, p < 0.0001, t = 14.93, df = 8; KCl/MK, p = 0.1940, t = 1.559, df = 4; unpaired t test; Figure S4C). The reduced NO emission in *kif5b*$^{+/-}$ slices might be caused by altered NO production machinery due to reduced kinesin-1, rather than by reduced NMDAR-mediated calcium influx. To exclude this possibility, we first performed a western blot analysis of neuronal NOS (nNOS) in wild-type and *kif5b*$^{+/-}$ slices, which showed identical amounts in both genotypes (p = 0.3579, t = 0.9689, df = 9; unpaired t test; Figure S2C). Next, we treated wild-type and *kif5b*$^{+/-}$ slices with A23187 (10 μM), which again showed similar NO emissions between genotypes (p = 0.9155, t = 0.1095, df = 8; unpaired t test; Figure S4C).

As it is known that extrasynaptic NMDAR activation would consequently lead to excitotoxicity, we tested whether the reduction of kinesin-1 would elicit neuroprotection against NMDA-induced excitotoxicity. The heterozygous knockout of *kif5b* gene had minimal impact on the viability of the neuronal culture, as the neuronal morphology was indistinguishable from that of its wild-type littermates. We treated the cortical cultures from both wild-type and *kif5b*$^{+/-}$ mice with NMDA (25–200 μM) and a co-agonist glycine (10 μM) for 10 min, which sufficed to induce neuronal death. After NMDA washout, cortical neurons were cultured for an additional 24 h. Cell death was examined by propidium iodide (PI) staining or by lactate dehydrogenase (LDH) assay, followed by morphological analysis under phase contrast microscopy. The *kif5b*$^{+/-}$ neurons treated with 100 μM NMDA and 10 μM glycine exhibited significantly fewer PI-positive neurons and less membrane leakage compared with the wild-type group (p = 0.0329, t = 2.758, df = 6; unpaired t test; Figures 4A and 4B; NMDA *kif5b*$^{+/+}$ vs. *kif5b*$^{+/-}$, p < 0.0001, t = 8.575,
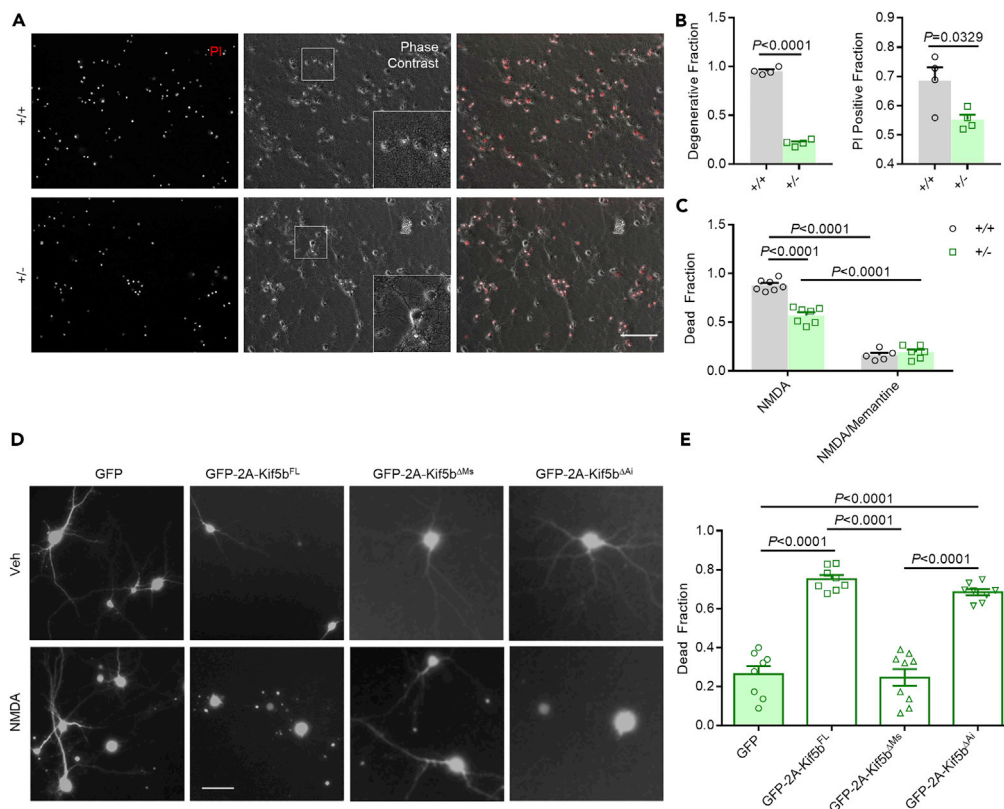
Figure 4. Kinesin-1 Reduction Protects Neuron against NMDA-Induced Excitotoxicity

(A and B) (A) Representative images and (B, left) quantification of PI-positive neurons and (B, right) degenerative neurons of wild-type (+/+) and $Kif5b^{+/-}$ (+/−) cultures (n = 4 per genotype, unpaired t test) after treatment with NMDA/glycine (Gly) for 10 min followed by washing for 24 h. The PI-positive fraction is the ratio of PI-positive neurons to PI-negative neurons, which indicates the portion of dead neurons. The degenerative fraction is the ratio of neurons with fragmented neurites to neurons with normal intact neurites, which indicates the portion of neurons with signs of early degeneration. Scale bar (white solid line), = 100 μm.

(C) Lactate dehydrogenase (LDH) leakage from NMDA-treated $kif5b^{+/-}$ (+/−) and wild-type (+/+) neurons (n = 7 for wild-type and n = 6 for $kif5b^{+/-}$ from three individual cultures, two-way ANOVA followed by Sidak *post hoc* test). The dead fraction is the ratio of LDH level in the drug-treated group to "all-kill" group.

(D and E) (D) Representative images and (E) quantification of dead and degenerative fractions of $kif5b^{+/-}$ cultures transfected with GFP, GFP-2A-Kif5b^{FL}, GFP-2A-Kif5b^{ΔMT}, and GFP-2A-Kif5b^{ΔAi} after treatment with NMDA/Gly or vehicle (Veh) for 10 min followed by washing for 24 h (n = 8 for each genotype from three individual cultures, unpaired t test). Scale bar (white solid line), 50 μm. Values are presented as mean ± SEM (test as indicated; exact p value given if less than 0.05).

df = 21; two-way ANOVA followed by Sidak *post hoc* test; Figure 4C). Morphologically, neurites in $kif5b^{+/-}$ neurons were mostly intact indicating significantly less early neurodegeneration, whereas most neurons in the wild-type group showed fragmented neurites indicating synaptic loss leading to early neurodegeneration (p < 0.0001, t = 30.37, df = 6; unpaired t test; Figures 4A and 4B). Although NMDA elicited neurotoxicity in both genotypes in a dose-dependent manner, the neurotoxic effects were significantly lower in $kif5b^{+/-}$ neurons at all tested concentrations (PI positive dose, $F_{(2,17)}$ = 22.34, p < 0.0001; degenerative dose, $F_{(2,17)}$ = 10.63, p = 0.0010; two-way ANOVA followed by Sidak *post hoc* test; Figures S4E and S4F). Moreover, treatment with memantine (50 μM), a potent NMDAR antagonist, significantly reduced NMDA-elicited neurotoxicity abolishing the differential neurotoxicity between $kif5b^{+/-}$ and wild-type neurons (genotype × memantine, $F_{(1,21)}$ = 38.64, p < 0.0001; NMDA/memantine +/+ versus +/−, p = 0.9797, t = 0.7228, df = 21; two-way ANOVA followed by Sidak *post hoc* test; Figure 4C). Furthermore, selective inhibition of extrasynaptic NMDAR by a low dose of memantine (1 μM) (Okamoto et al., 2009) and GluN2B-specific inhibitor Ro25-6981 (5 μM) produced similar levels of NMDA-induced neurotoxicity in both wild-type and $kif5b^{+/-}$ neurons (Mem, p = 0.4627, t = 0.7637, df = 10; Ro25, p = 0.7127,

t = 0.3789, df = 10; unpaired t test; Figure S4G). As the control experiments, kainate (25 μM), a non-NMDA excitotoxin, produced similar neurotoxicity in *kif5b*$^{+/-}$ and wild-type neurons (p = 0.4883, t = 0.7195, df = 10; unpaired t test; Figure S4H). Treatment with A23187, a calcium ionophore that increases the calcium-channel-independent level of intracellular calcium, elicited similar neurotoxicity in both genotypes (p = 0.8807, t = 0.1533, df = 12; unpaired t test; Figure S4H), indicating that kinesin-1-reduction-elicited neuroprotection is selective to NMDAR, at least in part, by preventing extra-synaptic NMDAR targeting and functioning.

To exclude the possibility that the reduced vulnerability to NMDA by reduced kinesin-1 level was due to secondary adaptation rather than the kinesin-1 reduction itself, we transiently overexpressed Kif5b with GFP separated by a 2A peptide in *kif5b*$^{+/-}$ neurons. After NMDA treatment, *kif5b*$^{+/-}$ neurons transfected with GFP had well-preserved morphology with robust neurites, whereas neurons transfected with the full-length Kif5b-2A-GFP displayed shrunken nuclei with significant loss of neurites (p < 0.0001, t = 10.59, df = 14; unpaired t test; Figures 4D and 4E). Moreover, we assessed the NMDA-elicited cell death in *kif5b*$^{+/-}$ neurons expressing either Kif5b with microtubule sliding site deletion or Kif5b with autoinhibitory site deletion. Transfection of either Kif5b mutants did not lead to spontaneous neurodegeneration (Figures 4D and 4E), as revealed by the intact neuronal morphology. We found that only Kif5b with autoinhibitory site deletion had enhanced neuronal susceptibility to NMDA-elicited neurotoxicity, as shown by significantly more fragmented neurites (p < 0.0001, t = 9.079 df = 15; unpaired t test; Figures 4D and 4E). These results confirm that the neuroprotection observed in *kif5b*$^{+/-}$ neurons was due to a direct kinesin-1-mediated cellular mechanism, possibly associated with intracellular transportation.

To examine if the kinesin-1 reduction would affect neuronal fate following noxious insult *in vivo*, we performed bilateral cerebral carotid artery occlusion (BCCAO) for 20 min on *kif5b*$^{+/-}$ and wild-type mice. The *kif5b*$^{+/-}$ mice were viable and fertile with no growth retardation (Genotype × time, male, F(5,18) = 0.05272, p = 0.9980, female, F(5,42) = 1.088, p = 0.3813; two-way ANOVA; Figure S5A) and no signs of spontaneous neurodegeneration, as seen by the similar gross hippocampal anatomy in both genotypes (Figure S5B). The induced transient global ischemia triggered robust neurodegeneration in the hippocampus (Tu et al., 2010). At 7 days after reperfusion, brain sections examined by TUNEL assay showed severe neuronal damage in the wild-type mice but only mild to moderate damage in the *kif5b*$^{+/-}$ mice. There was a significant increase in TUNEL-positive signals detected in wild-type hippocampal CA1 and CA3 regions (CA1, p < 0.0001, t = 6.0483, df = 36; CA3, p < 0.0001, t = 10.7425, df = 22; unpaired t test; Figures S5C and S5D). Next, we performed middle cerebral artery occlusion (MCAO) for 120 min on *kif5b*$^{+/-}$ and wild-type mice to induce focal cerebral ischemia (Lo et al., 2005; Tu et al., 2010). Consistent with BCCAO, we observed significantly improved neurological scores and reduced infarct volume in the *kif5b*$^{+/-}$ mice (Genotype, F (1, 11) = 13.88, p = 0.0033; two-way repeated measures ANOVA followed by Sidak *post hoc* test; infarct volume, p = 0.0014, t = 4.256, df = 11; unpaired t test; neurological score, U = 6.000, p = 0.0408, Mann-Whitney rank-sum test; Figures 5A–5D).

To examine the possibility that the observed neuroprotective phenotype in *kif5b*$^{+/-}$ mice is directly due to kinesin-1 reduction rather than developmental adaptation *in vivo*, we generated a conditional knockout model by crossing *kif5b*$^{fl/+}$ mice with Camk2a-Cre mice by *kif5b* excision starting in the third postnatal week to mimic postnatal Kif5b reduction, which should minimize developmental alteration caused by *kif5b* deletion (Tsien et al., 1996). As Camk2a-Cre mediates recombination only in a subset of excitatory neurons in the forebrain, it was not surprising to observe a modest reduction of Kif5b protein level at 6 weeks of age in both *kif5b*$^{fl/+}$;Camk2a-Cre and *kif5b*$^{fl/fl}$;Camk2a-Cre mice (F (2,6) = 4.925, p = 0.0543; one-way ANOVA; Figure S5E). However, immunohistochemistry for Kif5b in the CA1 region, where Camk2a-Cre has the most impact, revealed a robust reduction in Kif5b protein level in *kif5b*$^{fl/+}$;Camk2a-Cre mice when compared with their wild-type littermates (Figure S5F). These data confirm that Kif5b was reduced at 6 weeks age in a subset of neurons in the conditional knockout model. Consistent with our observation in *kif5b*$^{+/-}$ mice, the Camk2a-Cre-mediated conditional *kif5b* knockout mice showed robust resistance to MCAO-induced neurodegeneration (F, genotype, F (1, 10) = 16.20, p = 0.0024, two-way repeated measures ANOVA; g, p = 0.0051, t = 3.565 df = 10; unpaired t test; Figures 5E–5G). Moreover, we observed a significant increase in NeuN immunoreactivity in the CA1 region of *kif5b* conditional knockout mice after 2-h MCAO and 24-h reperfusion when compared with their wild-type littermates (p = 0.0022; Mann-Whitney test; Figures S5G and S5H). These combined results show that kinesin-1 reduction protects neurons against NMDAR-elicited excitotoxicity and ischemia-induced neurodegeneration.
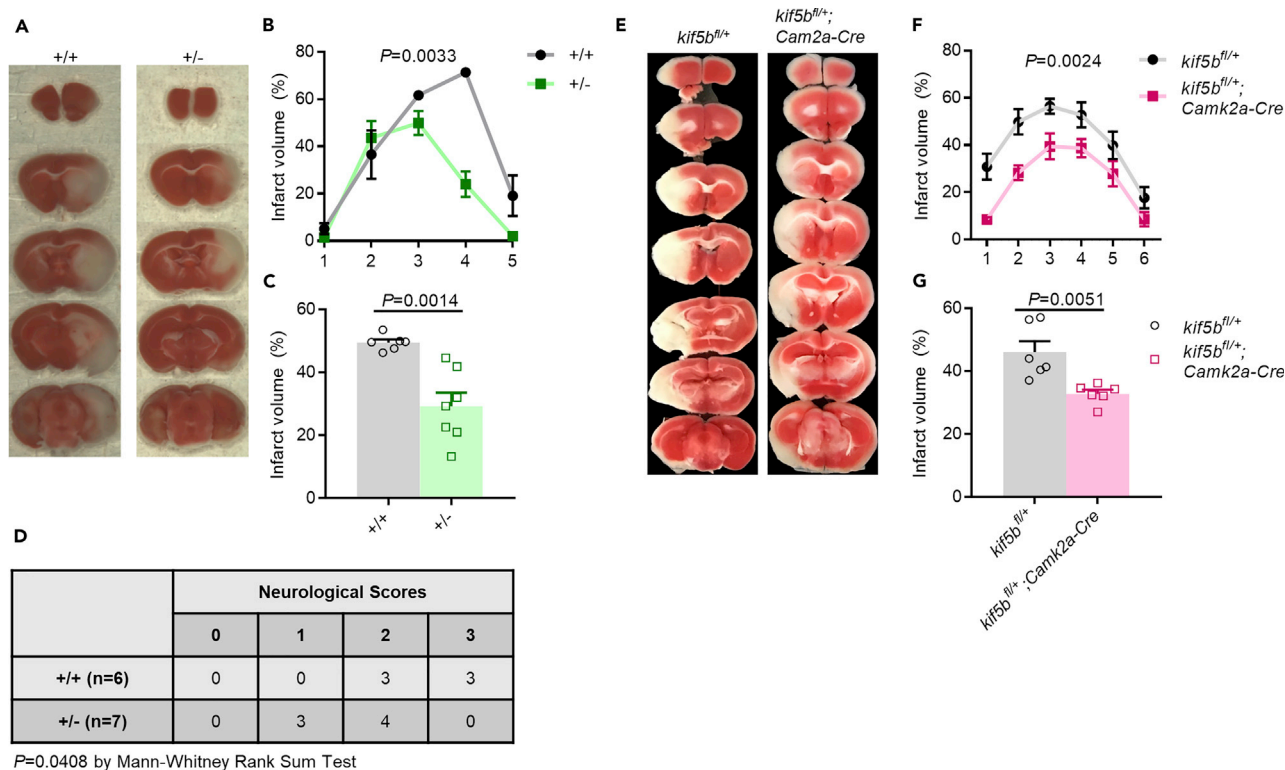
Figure 5. Kinesin-1 Reduction Protects Brain against Ischemia-Evoked Neurodegeneration

(A–C) (A) Representative images and (B and C) quantification of 2,3,5-triphenyltetrazolium chloride (TTC) staining of wild-type and kif5b^{+/−} mice after transient focal cerebral ischemia. Infarct volume of (B) the indicated slices and (C) whole brain (n = 6 for wild-type and n = 7 for kif5b^{+/−} mice; B, two-way ANOVA followed by Sidak *post hoc* test; C, unpaired t test).

(D) Neurological scoring revealed kif5b^{+/−} (+/−) mice had significant improvement in motor function after 2-h ischemia and 24-h reperfusion when compared with their wild-type littermates (+/+). (Neurological score: 0, freely moving; 1, reduced mobility; 2, partial paralysis; 3, no movement) (Mann-Whitney rank-sum test).

(E–G) (E) Representative images and (F and G) quantification of TTC staining of kif5b^{fl/+} and kif5b^{fl/+};Camk2a-Cre mice after MCAO. Infarct volume for indicated slices (F) and whole brain (G) (n = 6 for kif5b^{fl/+} and kif5b^{fl/+};Camk2a-Cre, respectively; F, two-way ANOVA followed by Sidak *post hoc* test; G, unpaired t test). Values are presented as mean $\pm$ SEM, unless otherwise indicated (test as indicated; exact p value given if less than 0.05).

Reduction of Kif5b Expression Associated with Suppression of Cell Death Pathways

Ischemia preconditioning (IPC) elicited neural-activity-dependent neuroprotection by altering the transcriptome to adapt to and resist subsequent noxious insult (Stenzel-Poore et al., 2003). As previous findings show a robust neuroprotective effect by kinesin-1 reduction, we hypothesized that the alteration of kinesin genes, particularly kinesin-1, might be a core mechanism underlying the IPC-elicited neuroprotection. To test this, we analyzed a microarray dataset (GEO:GSE32529) that profiled gene expressions at 3, 24, and 72 h after cerebral ischemia preconditioning (IPC) by a 15-min occlusion of middle cerebral artery in mice. Significantly altered genes at 3, 24, and 72 h after IPC were filtered and analyzed by Ingenuity Pathway Analysis platform (Qiagen) and compared with sham control groups (Figure 6A). By combining and comparing results from the "Diseases and Functions" analysis at the three indicated time points, we found that a set of genes relating to apoptosis and cell death were robustly enriched at 3 h after IPC, whereas this set of genes was suppressed at 24 and 72 h after IPC (Figure 6B). The finding of enhanced genes relating to apoptosis and cell death at 3 h after IPC was unexpected, and the overall trend supports the notion that brief exposure to IPC reprograms gene expression to protect the brain against lateral noxious insult. Besides the expected trends of inhibited cell death pathways or genes at the extended times after IPC, we unexpectedly identified suppressed genes related to neurodevelopment at over 3 to 72 h (Figure 6B). This raises the possibility that the same set of genes that regulate neurodevelopment also plays a key role in mediating neuronal adaptation to stress, including noxious insult. Kinesin genes plays a critical role in the development of cells and tissues such as neurons, muscles, chondrocytes, and osteoblasts (Hsu et al., 2011; Muhia et al., 2016; Padamsey et al., 2017; Qiu et al., 2012; Wang et al., 2013). We therefore
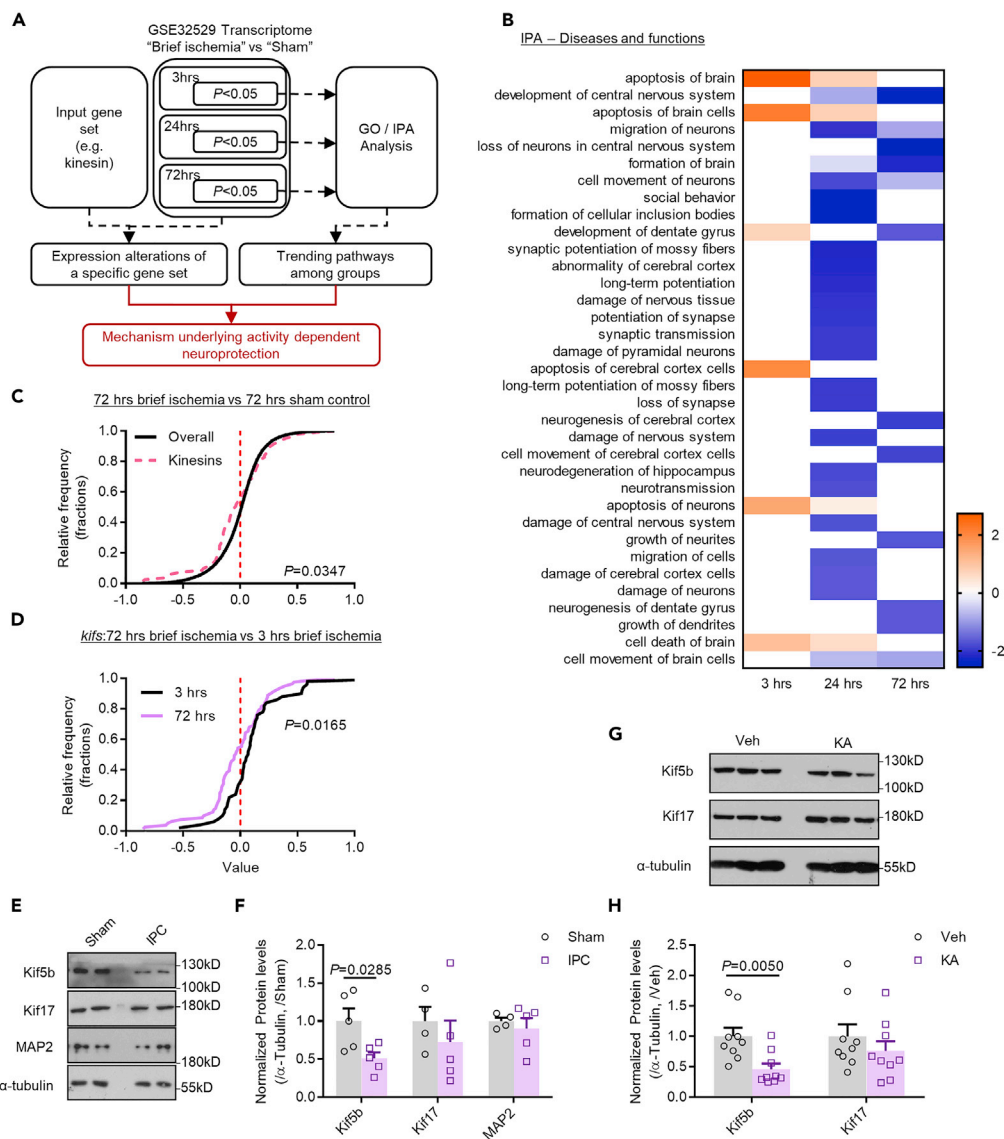
Figure 6. Transcriptome Analysis of Mouse Cortex after Ischemia Preconditioning Reveals that the Suppression of Cell Death Pathways Is Associated with Reduced *kif5b* Expression

(A) Schematic figure of the transcriptome analysis. The genes significantly altered at 3, 24, or 72 h after brief cerebral ischemia preconditioning (IPC) were analyzed by Ingenuity Pathway Analysis (IPA) platform. The expression of kinesin genes (*kifs*) were extracted and compared with the overall expression profile.

(B) IPA results of the pathways categorized by diseases and functions.

(C) The expression profiling of kinesin genes (*kifs*) were compared with the overall gene expression profile at 72 h after IPC normalized to 72 h in the sham control (Kolmogorov-Smirnov test).

(D) The expression profiling of kinesin genes at 3 and 72 h after IPC (Kolmogorov-Smirnov test).

(E and F) (E) Representative western blot images and (F) quantification of Kif5b, Kif17, and MAP2 in the hippocampus of wild-type mice after IPC or sham operation (n = 5 for the IPC group and n = 4 for the sham operation group, unpaired t test).

(G) Representative western blot image and (H) quantification of Kif5b, Kif17, and MAP2 in the hippocampus of wild-type mice with kainate treatment (KA, 12 mg/kg, 2 h) or vehicle (n = 9 for the KA group and n = 9 for the vehicle group, unpaired t test). Values are presented as mean ± SEM (test as indicated; exact p value given if less than 0.05).

investigated the global expression profile of kinesin genes at 3, 24, and 72 h after IPC in mice compared with the sham control group. The cumulative distribution of kinesin genes in the differentially expressed population exhibited a robust shift toward upregulation at 3 h, but not 24 h, after IPC (left, D = 0.2779,

p = 0.0009, Kolmogorov-Smirnov test; right, D = 0.1387, p = 0.0891; Kolmogorov-Smirnov test; Figure S6A). In contrast, the cumulative distribution of kinesin genes exhibited a significant shift toward downregulation at 72 h compared with the overall gene expression profile (D = 0.1583, p = 0.0347; Kolmogorov-Smirnov test; Figure 6C). This became more apparent when comparing the cumulative expression profile of kinesin genes at 3 and 72 h, which showed a significant downregulation shift (D = 0.2785, p = 0.0165, Kolmogorov-Smirnov test; Figure 6D). The results of the cumulative expression profile of kinesin genes suggests a time-dependent downregulation shift after IPC, which might indicate a kinesin-dependent mechanism underlying IPC-induced adaptation and neuroprotection. To identify which kinesin is the key player, we extracted probes for kinesin genes that were robustly altered at 72 h after IPC, which revealed two probes for *kif5b*. Moreover, we found that *kif5b* and *kif1b*, but not *kif3a*, were robustly repressed at 72 h compared with 3 h after IPC (*kif5b*, p = 0.0313; *kif1b*, p = 0.0313; *kif3a*, p = 0.1250; Wilcoxon matched-pairs signed rank test; Figure S6B), suggesting that the repression of *Kif5b* gene was a candidate event regulating neuronal adaptation to further ischemia insult.

To validate the transcriptome analysis, we first examined the expression levels of transport-related protein expression in mouse IPC model induced by a 15-min occlusion of middle cerebral artery. At 48 h after reperfusion, the level of Kif5b, the heavy chain of the microtubule-dependent motor kinesin-1, was significantly reduced (p = 0.0069, t = 3.605, df = 8, unpaired t test). However, levels of Kif17 and microtubule-associated protein-2 (MAP2), a component of neuron microtubule, were not changed (Kif17, p = 0.4703, t = 0.7632, df = 7; MAP2, p = 0.5731, t = 0.5910, df = 7; unpaired t test; Figures 6E and 6F). Next, we tested whether downregulation of Kif5b was specific to IPC or whether this was a response to the global regulation of neuronal activity. We injected mice with kainite to induce temporal lobe epilepsy and enhance neuronal activity (Ramamoorthi et al., 2011). We found that the level of Kif5b, but not Kif17, was reduced at 48 h after kainate treatment (Kif5b, p = 0.005, t = 3.2533, df = 16; Kif17, p = 0.3552, t = 0.9522, df = 16; unpaired t test; Figures 6G and 6H), which indicates that the reduction of kinesin-1 was associated with increased neuronal activity. This suggests a role of the intracellular transportation system underlying the suppression of cell death pathways by IPC and indicates that kinesin-1-dependent alteration of NMDAR compartmentalization might be the core mechanism.

DISCUSSION

The present study revealed a complex between kinesin-1 and GluN2B-containing NMDARs. This complex mediates the extrasynaptic targeting of NMDARs, the resulting pro-death signaling including calcium influx and NO production, and eventually neuronal vulnerability to NMDA-induced excitotoxicity and ischemia-evoked neurodegeneration. The transcriptome of IPC further implicates a role of kinesin-1 in mediating activity-dependent neuroprotection, probably via altering NMDAR compartmentalization and shifting the balance to highlight pro-survival pathways. Our findings demonstrate a role of kinesin-1 in mediating the compartmentalization of signaling pathways within neurons, which can be tuned down by suppressing kinesin-1 expression or by dissociating the interaction between kinesin-1 and GluN2B containing NMDAR when neurons sense a detrimental insult.

It has long been known that hyperactivation of NMDARs contribute to excitotoxicity and neuronal death. NMDAR-related excitotoxicity also acts as the major mechanism that causes neuronal death in both acute and chronic neurodegenerative disorders. However, attempts to translate NMDAR antagonization to clinical applications are far from satisfactory (De Keyser et al., 1999). The reasons might stem from the complexity of NMDAR-mediated signaling and subcellular compartmentalization (Zhou and Sheng, 2013). There are two distinct pools of NMDAR: synaptic NMDAR steadily accumulates at the PSD, whereas extrasynaptic NMDAR is more mobile and dynamic in extrasynaptic regions (Bading, 2017; Paoletti et al., 2013; Tovar and Westbrook, 1999). The downstream signaling and the functional consequence of these two distinct pools of NMDAR are also different. The activation of synaptic NMDAR activates mitogen-activated protein kinase signaling and modulates synaptic strength (Thomas and Huganir, 2004). The dysfunction of this pathway causes not only learning and memory deficits but also neuropsychiatric disorders such as schizophrenia (Cohen et al., 2015). The activation of synaptic NMDAR elicits the calcium-elicited pro-survival pathway (Hardingham et al., 2002). Our knowledge of extrasynaptic NMDAR is far less thorough compared with our understanding of synaptic NMDAR. The activation of extrasynaptic NMDAR was found to suppress the pro-death pathway mediated by synaptic NMDAR, which shifts the balance toward cell death in neurons. Furthermore, DARK1 is recruited to GluN2B and mediates the pro-death signaling toward excitotoxicity (Tu et al., 2010), whereas PGC-1α opposes extrasynaptic NMDAR function (Puddifoot et al., 2012).

One major question in this field is how the compartmentalization of signaling is regulated. Previous evidence indicates that extrasynaptic NMDARs are more mobile than the synaptic NMDARs (Groc et al., 2004), which makes the convergence of different transportation systems possible. In support of this notion, dynamin-dependent regulation is known to limit extrasynaptic synaptic activation (Wild et al., 2014). Our finding that microtubule-dependent transportation regulates extrasynaptic NMDAR fits into the current model in two ways. First, kinesin-1 may directly convey GluN2B-containing NMDAR to the extrasynaptic region. Kinesin-1 has been known to directly interact with Myosin Va (Huang et al., 1999), suggesting cooperation between microtubule- and actin-dependent transportation. Besides synaptic regions, actin filament dynamics are found to be enriched at the lateral zone and neck of the spine (Frost et al., 2010). Our model suggests that extrasynaptic NMDAR is first conveyed and targeted to extrasynaptic regions by microtubule-dependent transport and then moves between synaptic and extrasynaptic regions through the cooperation of microtubule- and actin-dependent transport systems. Second, kinesin-1 may convey internalized NMDAR from synaptic to extrasynaptic regions (Du et al., 2016). This is supported by the evidence that internalized NMDARs contain vesicles that are attached to microtubule-like filaments (Tovar and Westbrook, 1999), which further indicates a role of kinesin-1 in determining the fate of the internalized vesicles toward recycling or degradation.

Our finding that kinesin-1 mediates transport of NMDAR adds complexity to the anterograde transport of NMDAR. It has been proposed that Kif17 drives NR2B-containing NMDA receptors to synaptic sites (Setou et al., 2000; Yin et al., 2011), which is in parallel with our observation that knockdown of Kif5b reduced only extrasynaptic targeting and functioning. It is widely recognized that neurons may use different transport systems to convey cargo to distinct sub-domains, at least in the case of mitochondria transport, which relies on both Kif5 and Kif1b (Nangaku et al., 1994; Wang and Schwarz, 2009). When reaching the site with high levels of calcium, the mitochondrial membrane protein Miro mediates detachment or folding of kinesin-1, which traps the mitochondria (Wang and Schwarz, 2009), whereas Kif1b uses a KBP-dependent mechanism that is distinct from kinesin-1 (Wozniak et al., 2005). NMDAR exists as both diheteromer, consisting of GluN1/GluN2A or GluN1/GluN2B as the majority, or triheteromer consisting of GluN1/GluN2A/GluN2B in vivo. The functional properties of these two forms of NMDAR are different (Hansen et al., 2014). The triheteromer is presumably the dominant form of NMDAR in the adult forebrain, consistent with our data showing that kinesin-1 co-immunoprecipitates with both GluN2B and GluN2A (Figure 1A). However, it has also been reported that GluN2B containing NMDAR is the major form of NMDAR in the extrasynaptic site (Tovar and Westbrook, 1999). It is plausible that kinesin-1 has greater affinity to the diheteromer consisting of GluN1/GluN2B, which therefore enriches GluN2B-containing NMDAR in the extrasynaptic region, whereas the Kif17 has a greater impact on triheteromer, which is enriched in the synaptic region. Supporting this notion, our analysis on the surface distribution NMDAR reveals the reduction of GluN2B, but not GluN2A, in the surface (Figures 1G and 1H). To understand the function and compartmentalization of NMDARs in more detail, especially its role in activity-dependent plasticity and disease pathology, we need to examine the regulatory or coordinating mechanisms among the different kinesins and between different transportation systems.

It is well established that the hierarchical assembly of synapses and neuronal contacts is highly dependent on intracellular transportation systems (Hirokawa et al., 2010). Our findings provide an intrinsic-activity-dependent mechanism for the regulation of NMDARs, which protects neurons against excitotoxic insult. Reduction of NMDAR activity could be regarded as a form of protective feedback that limits excess NMDAR-dependent calcium influx triggering excitotoxicity. This feedback can be through a number of factors, such as NMDAR subunit composition (Martel et al., 2012), the association of scaffolding proteins (Forder and Tymianski, 2009), and neuronal activity (Groc et al., 2004; Wild et al., 2014). Furthermore, our findings combine and unify the associations between kinesin level, elicited neuroprotection, and subsequent impact on extrasynaptic NMDAR, which supports the notion that regulating components beyond the synapse might be essential to induce neuroprotection. Consistent with our current findings, reduced mTORC1 activity and the resulting induction of autophagy has been proposed as another neuronal-activity-dependent mechanism to induce tolerance. Interestingly, this mechanism might function closely with intracellular transportation systems in eliciting neuroprotection (Fu et al., 2014; Papadakis et al., 2013). Altogether, these findings provide a potential therapeutic strategy that could delay degenerative processes by extending the period and effect of intrinsic neuroprotective mechanisms.

Inhibiting kinesin has been proposed as a promising approach to treating cancer, and some small molecules have already been developed. For example, the Kif11 motor protein mediates mitosis and drives

glioblastoma invasion, proliferation, and self-renewal. Inhibition of Kif11 by a specific small molecule could stop the progression of glioblastoma (Venere et al., 2015). The perturbation of intracellular transport may not only treat malignant dividing cells such as cancer but also show promising effects on the central nervous system (CNS). Epothilone D, a microtubule stabilizer that can reduce microtubule dynamic and microtubule-dependent transport, was able to ameliorate the impaired exploratory behavior in a Rett mouse model (Delépine et al., 2016). Epothilone B, a US Food and Drug Administration-approved microtubule stabilizer that can limit microtubule-dependent transport, was able to reactivate neuronal polarization and promote axon regeneration after CNS injury (Ruschel et al., 2015).

Together with literatures, our findings suggest that targeting of intracellular transport, including kinesin-1, could be potential targets for deferring neurodegeneration. Extrasynaptic NMDAR has been implicated in both acute and chronic neurodegenerative diseases (Bading, 2017). This makes Kif5b/kinesin-1 a potential therapeutic candidate. Our study utilized an acute stroke model to examine the neuroprotective effect by reducing kinesin-1. It would be of translational interest to test the effect of kinesin-1 reduction on chronic neurodegenerative models, like those of Alzheimer and Parkinson diseases. Moreover, suppressing Kif5b expression, particularly by disrupting the Kif5b-GluN2B interaction, might open an alternate therapeutic avenue. As the structure for kinesin-1 cargo-binding motif has been resolved (Pernigo et al., 2013; Yip et al., 2016), it would be tempting to resolve the structure for kinesin-1-GluN2B complex and use this structure as the basis to predict or design molecules that could halt extrasynaptic NMDAR-mediated neurodegeneration. As such an approach would mimic intrinsic changes induced by brief and beneficial stimulations, it might be tolerated by brain and thus minimize potential side effects. This would also prolong the period before the brain becomes vulnerable to detrimental insult, enabling the brain to adapt or develop resistance (Stenzel-Poore et al., 2003), delay functional impacts like memory or motor deficits, and allow for efficient interventions (Armstead et al., 2018).

Limitations of the Study

We demonstrate that a panel of kinesin family proteins is reduced in the transcriptome of a mouse cerebral ischemia preconditioning model. Although our data show that Kif5b reduction is neuroprotective, the causal link between kinesin-1 reduction and ischemia-preconditioning-induced neuroprotection remains to be studied. Moreover, the current understanding of extrasynaptic NMDARs in physiological condition is still elusive. Although we find that the heterozygous knockout of *kif5b* gene reduces extrasynaptic NMDARs, but not synaptic ones, and the *kif5b*$^{+/-}$ mice appear to be tolerant, additional experiments are needed to characterize the physiology and behavioral states of neuronal kinesin-1 reduction *in vivo*.

METHODS

All methods can be found in the accompanying Transparent Methods supplemental file.

SUPPLEMENTAL INFORMATION

Supplemental Information can be found online at https://doi.org/10.1016/j.isci.2019.02.009.

AUTHOR CONTRIBUTIONS

The work presented here was carried out in collaboration with all authors. J.D.H. directed and coordinated the study. R.L. designed and conducted the experiments and analyzed the data. Z.D. performed the GST pull-down experiments and rescue experiments. J.W. performed the pilot experiments. M.-L.F., C.-F.L., and Y.L. conducted the NO measurements. D.Y., A.C.Y.L., H.C., H.S., and J. S. helped with the MCAO

REFERENCES

Armstead, W.M., Hekierski, H., Pastor, P., Yarovoi, S., Higazi, A.A.-R., and Cines, D.B. (2018). Release of IL-6 after stroke contributes to impaired cerebral autoregulation and hippocampal neuronal necrosis through NMDA receptor activation and upregulation of ET-1 and JNK. Transl. Stroke Res. 10, 1–8.

Bading, H. (2013). Nuclear calcium signalling in the regulation of brain function. Nat. Rev. Neurosci. 14, 593–608.

Bading, H. (2017). Therapeutic targeting of the pathological triad of extrasynaptic NMDA receptor signaling in neurodegenerations. J. Exp. Med. 214, 569–578.

Chu, Y., Morfini, G.A., Langhamer, L.B., He, Y., Brady, S.T., and Kordower, J.H. (2012). Alterations in axonal transport motor proteins in sporadic and experimental Parkinson's disease. Brain 135, 2058–2073.

Cohen, S.M., Tsien, R.W., Goff, D.C., and Halassa, M.M. (2015). The impact of NMDA receptor hypofunction on GABAergic neurons in the pathophysiology of schizophrenia. Schizophrenia Res. 167, 98–107.

De Keyser, J., Sulter, G., and Luiten, P.G. (1999). Clinical trials with neuroprotective drugs in acute ischaemic stroke: are we doing the right thing? Trends Neurosci. 22, 535–540.

Delépine, C., Meziane, H., Nectoux, J., Opitz, M., Smith, A.B., Ballatore, C., Saillour, Y., Bennaceur-Griscelli, A., Chang, Q., Williams, E.C., et al. (2016). Altered microtubule dynamics and vesicular transport in mouse and human MeCP2-deficient astrocytes. Hum. Mol. Genet. 25, 146–157.

Du, W., Su, Q.P., Chen, Y., Zhu, Y., Jiang, D., Rong, Y., Zhang, S., Zhang, Y., Ren, H., Zhang, C., et al. (2016). Kinesin 1 drives autolysosome tubulation. Dev. Cell 37, 326–336.

Forder, J.P., and Tymianski, M. (2009). Postsynaptic mechanisms of excitotoxicity: involvement of postsynaptic density proteins, radicals, and oxidant molecules. Neuroscience 158, 293–300.

Frost, N.A., Shroff, H., Kong, H., Betzig, E., and Blanpied, T.A. (2010). Single-molecule discrimination of discrete perisynaptic and distributed sites of actin filament assembly within dendritic spines. Neuron 67, 86–99.

Fu, M.M., Nirschl, J.J., and Holzbaur, E.L. (2014). LC3 binding to the scaffolding protein JIP1 regulates processive dynein-driven transport of autophagosomes. Dev. Cell 29, 577–590.

Groc, L., Heine, M., Cognet, L., Brickley, K., Lounis, B., and Choquet, D. (2004). Differential activity-dependent regulation of the lateral mobilities of AMPA and NMDA receptors. Nat. Neurosci. 7, 695–696.

Hansen, K.B., Ogden, K.K., Yuan, H., and Traynelis, S.F. (2014). Distinct functional and pharmacological properties of triheteromeric GluN1/GluN2A/GluN2B NMDA receptors. Neuron 81, 1084–1096.

Hardingham, G.E., Fukunaga, Y., and Bading, H. (2002). Extrasynaptic NMDARs oppose synaptic NMDARs by triggering CREB shut-off and cell death pathways. Nat. Neurosci. 5, 405–414.

Hirokawa, N., Niwa, S., and Tanaka, Y. (2010). Molecular motors in neurons: transport mechanisms and roles in brain function, development, and disease. Neuron 68, 610–638.

Hsu, S.-H.C., Zhang, X., Yu, C., Li, Z.J., Wunder, J.S., Hui, C.-C., and Alman, B.A. (2011). Kif7 promotes hedgehog signaling in growth plate chondrocytes by restricting the inhibitory function of Sufu. Development 138, 3791–3801.

Huang, J.-D., Brady, S.T., Richards, B.W., Stenoien, D., Resau, J.H., Copeland, N.G., and Jenkins, N.A. (1999). Direct interaction of microtubule- and actin-based transport motors. Nature 397, 267.

Kaan, H.Y., Hackney, D.D., and Kozielski, F. (2011). The structure of the kinesin-1 motor-tail complex reveals the mechanism of autoinhibition. Science 333, 883–885.

Lo, A.C., Chen, A.Y., Hung, V.K., Yaw, L.P., Fung, M.K., Ho, M.C., Tsang, M.C., Chung, S.S., and Chung, S.K. (2005). Endothelin-1 overexpression leads to further water accumulation and brain edema after middle cerebral artery occlusion via aquaporin 4 expression in astrocytic end-feet. J. Cereb. Blood Flow Metab. 25, 998–1011.

Martel, M.A., Ryan, T.J., Bell, K.F., Fowler, J.H., McMahon, A., Al-Mubarak, B., Komiyama, N.H., Horsburgh, K., Kind, P.C., Grant, S.G., et al. (2012). The subtype of GluN2 C-terminal domain determines the response to excitotoxic insults. Neuron 74, 543–556.

Molokanova, E., Akhtar, M.W., Sanz-Blasco, S., Tu, S., Piña-Crespo, J.C., McKercher, S.R., and Lipton, S.A. (2014). Differential effects of synaptic and extrasynaptic NMDA receptors on Aβ-induced nitric oxide production in cerebrocortical neurons. J. Neurosci. 34, 5023–5028.

Muhia, M., Thies, E., Labonté, D., Ghiretti, A.E., Gromova, K.V., Xompero, F., Lappe-Siefke, C., Hermans-Borgmeyer, I., Kuhl, D., Schweizer, M., et al. (2016). The kinesin KIF21B regulates microtubule dynamics and is essential for neuronal morphology, synapse function, and learning and memory. Cell Rep. 15, 968–977.

Nangaku, M., Sato-Yoshitake, R., Okada, Y., Noda, Y., Takemura, R., Yamazaki, H., and Hirokawa, N. (1994). KIF1B, a novel microtubule plus end-directed monomeric motor protein for transport of mitochondria. Cell 79, 1209–1220.

Okamoto, S., Pouladi, M.A., Talantova, M., Yao, D., Xia, P., Ehrnhoefer, D.E., Zaidi, R., Clemente, A., Kaul, M., Graham, R.K., et al. (2009). Balance between synaptic versus extrasynaptic NMDA receptor activity influences inclusions and neurotoxicity of mutant huntingtin. Nat. Med. 15, 1407–1413.

Padamsey, Z., McGuinness, L., Bardo, S.J., Reinhart, M., Tong, R., Hedegaard, A., Hart, M.L., and Emptage, N.J. (2017). Activity-dependent exocytosis of lysosomes regulates the structural plasticity of dendritic spines. Neuron 93, 132–146.

Paoletti, P., Bellone, C., and Zhou, Q. (2013). NMDA receptor subunit diversity: impact on receptor properties, synaptic plasticity and disease. Nat. Rev. Neurosci. 14, 383–400.

Papadakis, M., Hadley, G., Xilouri, M., Hoyte, L.C., Nagel, S., McMenamin, M.M., Tsaknakis, G., Watt, S.M., Drakesmith, C.W., Chen, R., et al. (2013). Tsc1 (hamartin) confers neuroprotection against ischemia by inducing autophagy. Nat. Med. 19, 351–357.

Pernigo, S., Lamprecht, A., Steiner, R.A., and Dodding, M.P. (2013). Structural basis for kinesin-1:cargo recognition. Science 340, 356–359.

Puddifoot, C., Martel, M.-A., Soriano, F.X., Camacho, A., Vidal-Puig, A., Wyllie, D.J.A., and Hardingham, G.E. (2012). PGC-1α negatively regulates extrasynaptic NMDAR activity and excitotoxicity. J. Neurosci. 32, 6995–7000.

Qiu, N., Xiao, Z., Cao, L., Buechel, M.M., David, V., Roan, E., and Quarles, L.D. (2012). Disruption of Kif3a in osteoblasts results in defective bone formation and osteopenia. J. Cell Sci. *125* (Pt 8), 1945–1957.

Ramamoorthi, K., Fropf, R., Belfort, G.M., Fitzmaurice, H.L., McKinney, R.M., Neve, R.L., Otto, T., and Lin, Y. (2011). Npas4 regulates a transcriptional program in CA3 required for contextual memory formation. Science *334*, 1669–1675.

Ruschel, J., Hellal, F., Flynn, K.C., Dupraz, S., Elliott, D.A., Tedeschi, A., Bates, M., Sliwinski, C., Brook, G., Dobrindt, K., et al. (2015). Systemic administration of epothilone B promotes axon regeneration after spinal cord injury. Science *348*, 347–352.

Sanacora, G., Frye, M.A., McDonald, W., Mathew, S.J., Turner, M.S., Schatzberg, A.F., Summergrad, P., and Nemeroff, C.B.; American Psychiatric Association (APA) Council of Research Task Force on Novel Biomarkers and Treatments (2017). A consensus statement on the use of ketamine in the treatment of mood disorders. JAMA Psychiatry *74*, 399–405.

Sattler, R., Xiong, Z., Lu, W.Y., Hafner, M., MacDonald, J.F., and Tymianski, M. (1999). Specific coupling of NMDA receptor activation to nitric oxide neurotoxicity by PSD-95 protein. Science *284*, 1845–1848.

Setou, M., Nakagawa, T., Seog, D.H., and Hirokawa, N. (2000). Kinesin superfamily motor protein KIF17 and mLin-10 in NMDA receptor-containing vesicle transport. Science *288*, 1796–1802.

Stenzel-Poore, M.P., Stevens, S.L., Xiong, Z., Lessov, N.S., Harrington, C.A., Mori, M., Meller, R., Rosenzweig, H.L., Tobar, E., Shaw, T.E., et al. (2003). Effect of ischaemic preconditioning on genomic response to cerebral ischaemia: similarity to neuroprotective strategies in hibernation and hypoxia-tolerant states. Lancet *362*, 1028–1037.

Stokin, G.B., Lillo, C., Falzone, T.L., Brusch, R.G., Rockenstein, E., Mount, S.L., Raman, R., Davies,

P., Masliah, E., Williams, D.S., et al. (2005). Axonopathy and transport deficits early in the pathogenesis of Alzheimer's disease. Science *307*, 1282–1288.

Tanaka, Y., Kanai, Y., Okada, Y., Nonaka, S., Takeda, S., Harada, A., and Hirokawa, N. (1998). Targeted disruption of mouse conventional kinesin heavy chain kif5B, results in abnormal perinuclear clustering of mitochondria. Cell *93*, 1147–1158.

Terenzio, M., Schiavo, G., and Fainzilber, M. (2017). Compartmentalized signaling in neurons: from cell biology to neuroscience. Neuron *96*, 667–679.

Thomas, G.M., and Huganir, R.L. (2004). MAPK cascade signalling and synaptic plasticity. Nat. Rev. Neurosci. *5*, 173–183.

Tjong, Y.W., Jian, K., Li, M., Chen, M., Gao, T.M., and Fung, M.L. (2007). Elevated endogenous nitric oxide increases Ca2+ flux via L-type Ca2+ channels by S-nitrosylation in rat hippocampal neurons during severe hypoxia and in vitro ischemia. Free Radic. Biol. Med. *42*, 52–63.

Tovar, K.R., and Westbrook, G.L. (1999). The incorporation of NMDA receptors with a distinct subunit composition at nascent hippocampal synapses in vitro. J. Neurosci. *19*, 4180–4188.

Tsien, J.Z., Chen, D.F., Gerber, D., Tom, C., Mercer, E.H., Anderson, D.J., Mayford, M., Kandel, E.R., and Tonegawa, S. (1996). Subregion- and cell type-restricted gene knockout in mouse brain. Cell *87*, 1317–1326.

Tu, W., Xu, X., Peng, L., Zhong, X., Zhang, W., Soundarapandian, M.M., Balel, C., Wang, M., Jia, N., Zhang, W., et al. (2010). DAPK1 interaction with NMDA receptor NR2B subunits mediates brain damage in stroke. Cell *140*, 222–234.

Venere, M., Horbinski, C., Crish, J.F., Jin, X., Vasanji, A., Major, J., Burrows, A.C., Chang, C., Prokop, J., Wu, Q., et al. (2015). The mitotic kinesin KIF11 is a driver of invasion, proliferation, and self-renewal in glioblastoma. Sci. Transl. Med. *7*, 304ra143.

Verhey, K.J., Kaul, N., and Soppina, V. (2011). Kinesin assembly and movement in cells. Annu. Rev. Biophys. *40*, 267–288.

Volk, L., Chiu, S.L., Sharma, K., and Huganir, R.L. (2015). Glutamate synapses in human cognitive disorders. Annu. Rev. Neurosci. *38*, 127–149.

Wang, X., and Schwarz, T.L. (2009). The mechanism of Ca2+-dependent regulation of kinesin-mediated mitochondrial motility. Cell *136*, 163–174.

Wang, Z., Cui, J., Wong, W.M., Li, X., Xue, W., Lin, R., Wang, J., Wang, P., Tanner, J.A., Cheah, K.S.E., et al. (2013). Kif5b controls the localization of myofibril components for their assembly and linkage to the myotendinous junctions. Development *140*, 617–626.

Wild, A.R., Jones, S., and Gibb, A.J. (2014). Activity-dependent regulation of NMDA receptors in substantia nigra dopaminergic neurones. J. Physiol. *592*, 653–668.

Wong, Y.L., and Rice, S.E. (2010). Kinesin's light chains inhibit the head- and microtubule-binding activity of its tail. Proc. Natl. Acad. Sci. U S A *107*, 11781–11786.

Wozniak, M.J., Melzer, M., Dorner, C., Haring, H.-U., and Lammers, R. (2005). The novel protein KBP regulates mitochondria localization by interaction with a kinesin-like protein. BMC Cell Biol. *6*, 35.

Yin, X., Takei, Y., Kido, M.A., and Hirokawa, N. (2011). Molecular motor KIF17 is fundamental for memory and learning via differential support of synaptic NR2A/2B levels. Neuron *70*, 310–325.

Yip, Y.Y., Pernigo, S., Sanger, A., Xu, M., Parsons, M., Steiner, R.A., and Dodding, M.P. (2016). The light chains of kinesin-1 are autoinhibited. Proc. Natl. Acad. Sci. U S A *113*, 2418–2423.

Zhou, Q., and Sheng, M. (2013). NMDA receptors in nervous system diseases. Neuropharmacology *74*, 69–75.

Supplemental Information

Kinesin-1 Regulates Extrasynaptic

Targeting of NMDARs and Neuronal
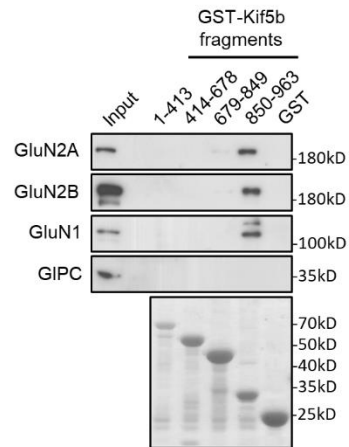
Vulnerability Toward Excitotoxicity

Raozhou Lin, Zhigang Duan, Haitao Sun, Man-Lung Fung, Hansen Chen, Jing Wang, Chi-Fai Lau, Di Yang, Yu Liu, Yanxiang Ni, Zai Wang, Ju Cui, Wutian Wu, Wing-Ho Yung, Ying-Shing Chan, Amy C.Y. Lo, Jun Xia, Jiangang Shen, and Jian-Dong Huang
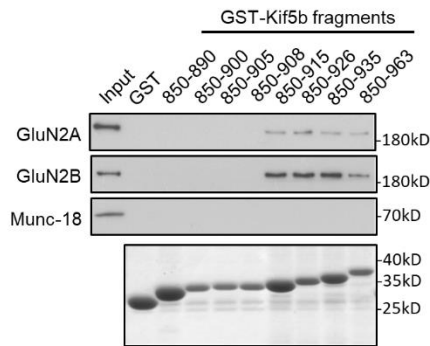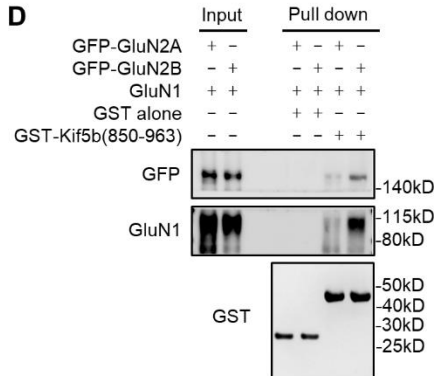
Supplemental Figures
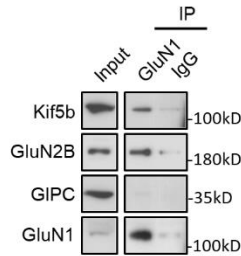
Figure S1 Kinesin-1 binds with GluN2B-containing NMDARs, related to Figure 1.

(A) Western blot of immunoprecipitated GluN1 from mouse brain lysate. GAIP-interacting protein C terminus (GIPC) is a neuronal PDZ protein. (B) and (C) Representative western blots of GST pull-down eluate from mouse brain lysate by GST-fused Kif5b fragments, as indicated. (D) Representative western blots of GST pull-down eluate from lysate of 293T cell with overexpressing GluN2A/GluN1 or GluN2B/GluN1.
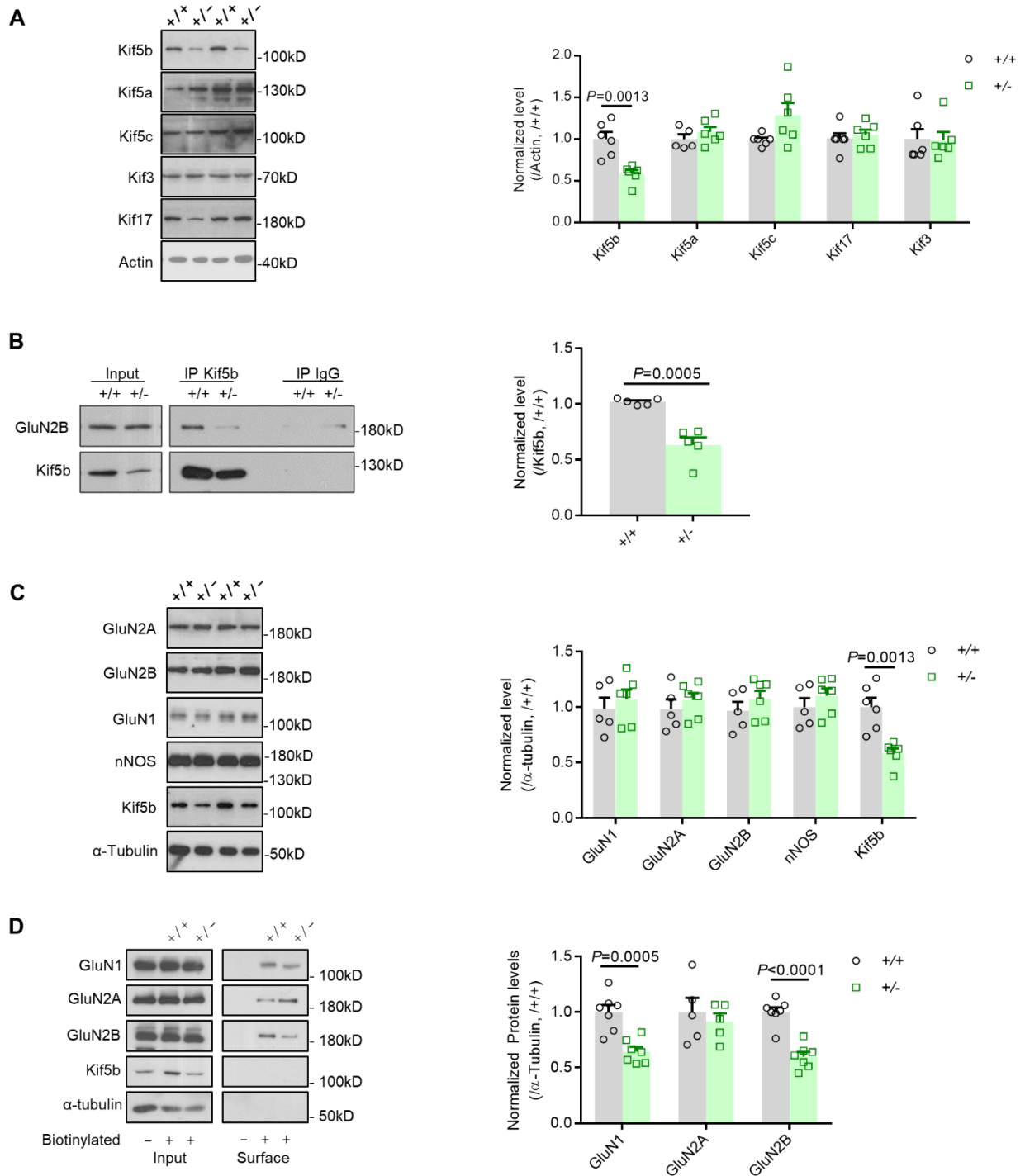
Figure S2 Reduced surface distribution of GluN2B-containing NMDARs in *kif5b*$^{+/-}$ mice, related to Figure 2.

(A) Representative Western blot images and quantification of Kif5b, Kif5a, Kif5c, Kif17, and Kif3 proteins in the hippocampus of the *kif5b*$^{+/-}$ (+/-) mice and their wild-type littermates (+/+). The intensities of blots were normalized to the internal control (α-tubulin) (n=5-6 mice per genotype; unpaired t-test). (B)

Representative Western blot images and quantification of Kif5b immunoprecipitation in $kif5b^{+/-}$ (+/-) mice and their wild-type (+/+) littermates. GluN2B levels were normalized to Kif5b in the Kif5b immunoprecipitation (n=5 mice per genotype; unpaired t-test). (C) Representatives Western blot images and quantification of GluN1, GluN2A, GluN2B, nNOS, Kif5b, and α-tubulin proteins in the hippocampus of $Kif5b^{+/-}$ (+/-) mice and their wild-type (+/+) littermates (n=6 mice per genotype; unpaired t-test). The intensities of blots were normalized to the internal control (α-tubulin). (D) Representative Western blot images and quantification of biotinylated surface GluN1, GluN2A, and GluN2B levels from acutely prepared hippocampal slices from $kif5b^{+/-}$ mice (+/-) and their wild-type littermates (+/+). Mixed genotype (mx) for the non-biotinylated control. The intensities of the blots from kif5b+/- mice were normalized to the loading control (n=7 for GluN1 and GluN2B per genotype, n=5 for GluN2A per genotype, from five individual experiments, paired t-test). Values are presented as mean ± s.e.m., unless otherwise indicated (test as indicated; exact P value given if less than 0.05).
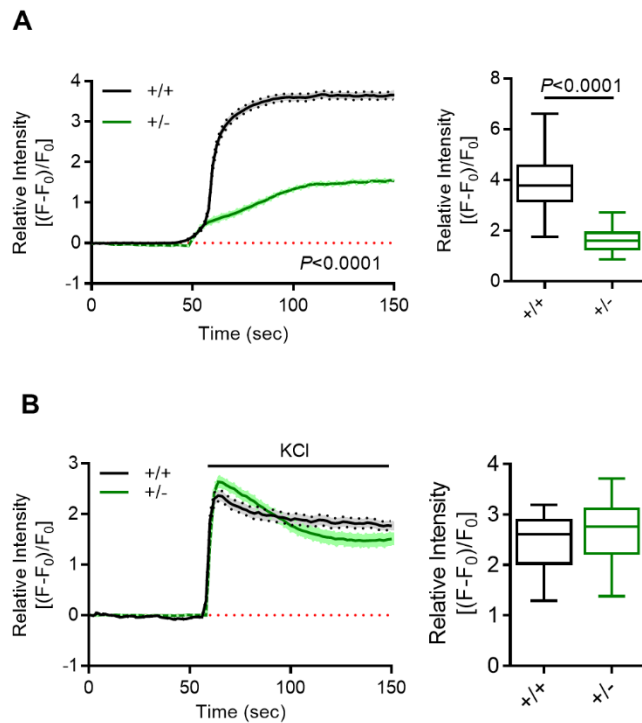
Figure S3 Reduced NMDAR dependent calcium influx in *kif5b^{+/-}* mice, related to Figure 3.

(A) Time-lapse and peak response of NMDA-induced calcium influx in *kif5b^{+/-}* (+/-) and wild-type (+/+) neurons (n=94 for wild-type and n=68 for *kif5b^{+/-}* from three individual experiments; scale bar = 20 μm; A, left, two-way ANOVA; A, right, Mann-Whitney U test). (B) Time-lapse and peak response of *kif5b^{+/-}* (+/-) and wild-type (+/+) neurons treated with KCl (70 mM). Calcium response was presented as the ratio $[(F-F_0)/F_0]$ of the Fluo-3 fluorescence intensity difference $(F-F_0)$ between the baseline and the indicated time point to baseline intensity (F_0) (n=27 for wild-type and n=28 for *kif5b^{+/-}*; B, left, two-way ANOVA; B, right, Mann-Whitney U test). Values are presented as mean ± s.e.m., unless otherwise indicated (test as indicated; exact *P* value given if less than 0.05).
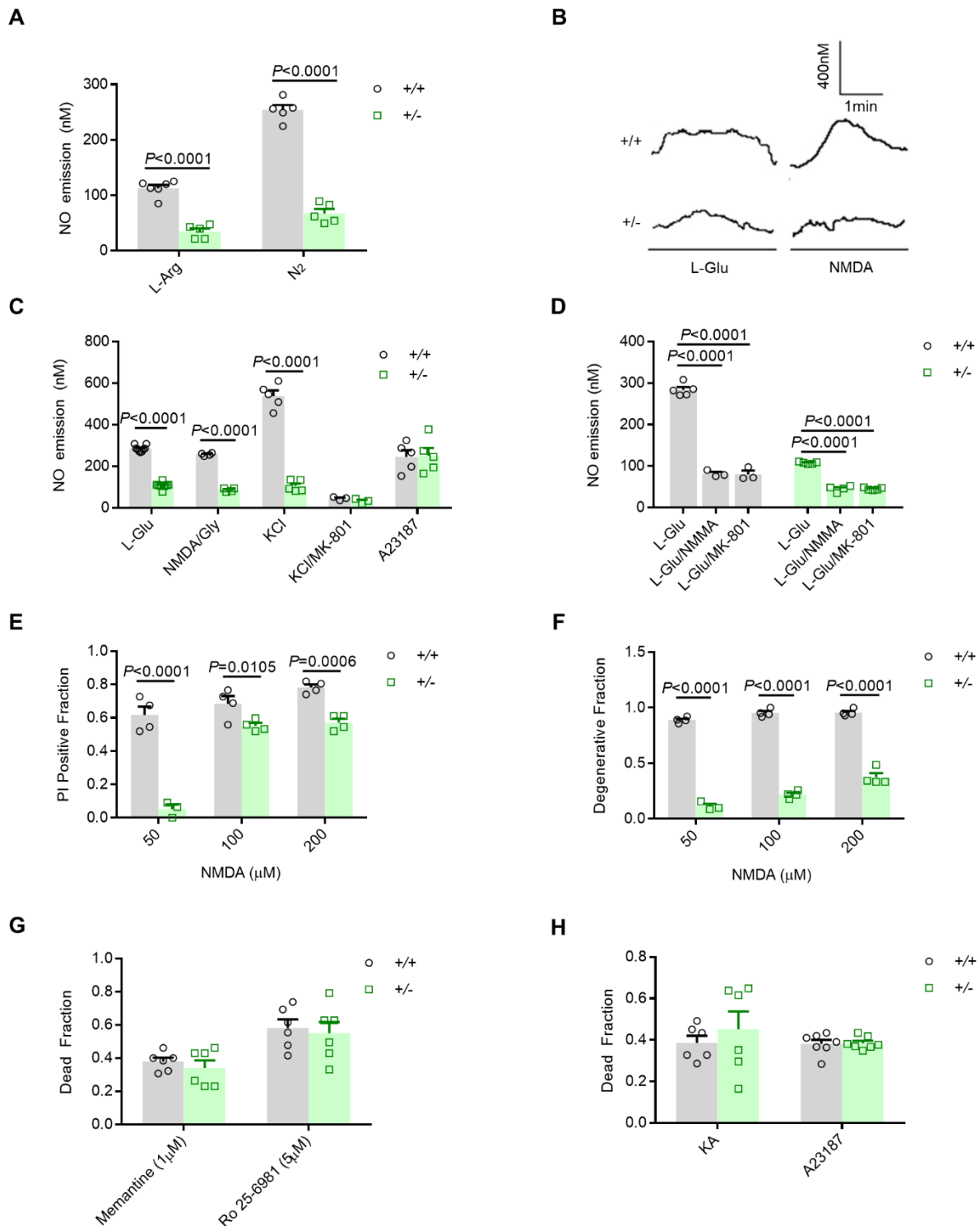
Figure S4 Reduced NMDA induced exicitotoxicity *kif5b*^{+/-} neurons, related to Figure 4.

(A) L-Arginine (L-Arg) and hypoxia (N$_2$) induced a differential response in NO emission of *kif5b*^{+/-} (+/-) and wild-type (+/+) slices (n=4-6 per genotype; unpaired t-test). (B) Representative curves and (C)

quantification of NO emission in the presence of different pharmacological agents (L-Glu, n=9 for wild-type, n=10 for *kif5b*$^{+/-}$; NMDA, n=4 for wild-type, n=4 for *kif5b*$^{+/-}$; KCl, n=5 for wild-type, n=5 for *kif5b*$^{+/-}$; KCl/MK-801, n=3 for wild-type, n=3 for *kif5b*$^{+/-}$; A23187, n=5 for wild-type, n=5 for *kif5b*$^{+/-}$; unpaired t-test). L-Glu and NMDA/Gly are agonists for NMDA-induced NO emission. KCl was used to depolarize the hippocampal slices, MK-801 was applied to block NMDAR calcium channels, and A23187 (a calcium ionophore) was used to increase the intracellular calcium level by bypassing the existing endogenous calcium channels. (D) MK-801 (100 µM) and L-NMMA (100 µM) highly suppressed NO emission in *kif5b*$^{+/-}$ (+/-) and wild-type (+/+) slices following glutamate (L-Glu, 4 µM) and glycine (20 µM) treatment (n=4-6 per genotype; unpaired t-test). (E) PI-positive neurons and (F) degenerative neurons of wild-type (+/+) and *kif5b*$^{+/-}$ (+/-) cultures were quantified after treatment with NMDA (concentrations as indicated) for 10 min followed by washing for 24 hrs (n=3-6 per genotype; two-way ANOVA followed by Sidak post hoc test). (G) LDH leakage from *kif5b*$^{+/-}$ (+/-) and wild-type (+/+) neurons treated with kainate (KA, n=6 per genotype; unpaired t-test) or A23187 (n=7 per genotype; unpaired t-test) overnight. (H) LDH leakage from NMDA-treated *kif5b*$^{+/-}$ (+/-) and wild-type (+/+) neurons (n=3-6 per genotype) in the presence of memantine (1 µM) or Ro25-6981 (5 µM) (n=6 per treatment per genotype, unpaired t-test). Values are presented as mean $\pm$ s.e.m., unless otherwise indicated (test as indicated; exact P value given if less than 0.05.)
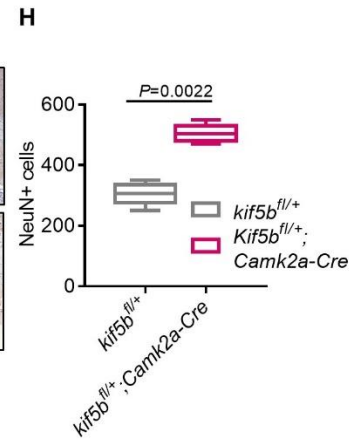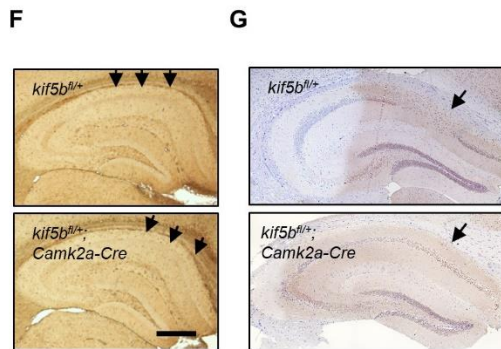
A

Male

+/+
+/−

Body weight (g)

Days post birth

Female

+/+
+/−

Body weight (g)

Days post birth

B

| H&E | Nissl | NeuN | NF-H | GFAP |

+/+

+/−

C

CA1

+/+   +/−

CA3

+/+   +/−

TUNEL

DAPI

D

+/+
+/−

TUNEL+ cells (per 2500μm²)

P<0.0001

P<0.0001

CA1   CA3

E

Kif5b^{fl/fl}   *Kif5b^{fl/+};Camk2a-Cre*   *Kif5b^{fl/fl};Camk2a-Cre*

Kif5b   100kD
Actin   37kD

Normalized Protein levels (/Actin, /*kif5b^{fl/+}*)

kif5b^{fl/+}   *kif5b^{fl/+};Camk2a-Cre*   *kif5b^{fl/fl};Camk2a-Cre*

F

kif5b^{fl/+}

kif5b^{fl/+}; Camk2a-Cre

G

kif5b^{fl/+}

kif5b^{fl/+}; Camk2a-Cre

H

P=0.0022

NeuN+ cells

kif5b^{fl/+}
Kif5b^{fl/+}; Camk2a-Cre

kif5b^{fl/+}   *kif5b^{fl/+};Camk2a-Cre*

Figure S5 Reduced cerebral ischemia induced neurodegeneration in *kif5b$^{+/-}$* mice, related to Figure 5.

(A) *kif5b$^{+/-}$* (+/-) mice and their wild-type (+/+) littermates were weighed from day 20 after birth (n=5 for male/genotype; n=9 for female/genotype; two-way ANOVA followed by Sidak post hoc test). (B) Paraffin sections of hippocampi from *kif5b$^{+/-}$* (+/-) mice and their wild-type (+/+) littermates were stained with hematoxylin and eosin (H&E) and cresyl violet (Nissl). Immunohistochemistry of neuronal nuclei (NeuN), neurofilament heavy chains (NF-H) and astrocyte markers (GFAP). Scale bar (black solid line) = 500 μm. (C) Representative images and (D) quantification of the TUNEL assay in wild-type and *kif5b$^{+/-}$* mice after transient global ischemia. CA1 (left) and CA3 (right) regions of the hippocampus are shown. Blot plots indicate the range from max to min (three fields per region per mouse; n=4 per genotype; Mann-Whitney U test; scale bars = 50 μm). (E, upper) Representatives Western blot images and (lower) quantification of Kif5b and Actin protein levels in the forebrain of *kif5b$^{fl/+}$*, *kif5b$^{fl/+}$;Camk2a-Cre*, and *kif5b$^{fl/fl}$;Camk2a-Cre* mice (n=3 for each genotype, one-way ANOVA followed by Holm-Sidak's multiple comparisons post hoc test). (F) Immunohistochemistry of Kif5b in the hippocampus of *kif5b$^{fl/+}$* and *kif5b$^{fl/+}$;Camk2a-Cre* mice (scale bars = 50 μm, black solid line). (G) Representative image and (H) quantification of the immunohistochemistry of NeuN on *kif5b$^{fl/+}$* and *kif5b$^{fl/+}$;Camk2a-Cre* mice after 2 hrs of cerebral ischemia and 24 hrs of reperfusion (n=6 per genotype; Mann-Whitney U test; scale bars = 50 μm). Values are presented as mean ± s.e.m., unless otherwise indicated (test as indicated; exact *P* value given if less than 0.05).

A
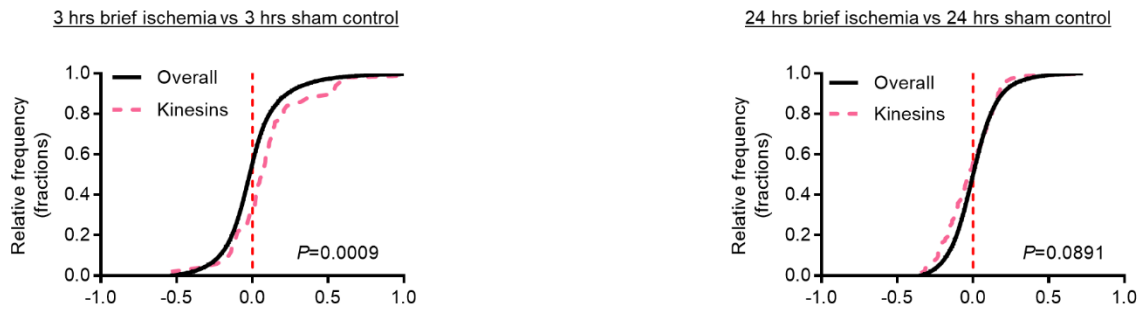
B

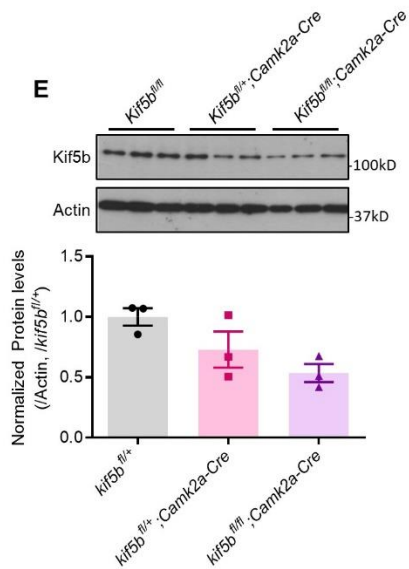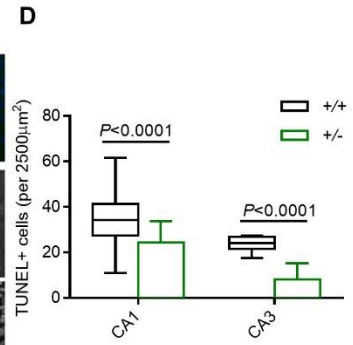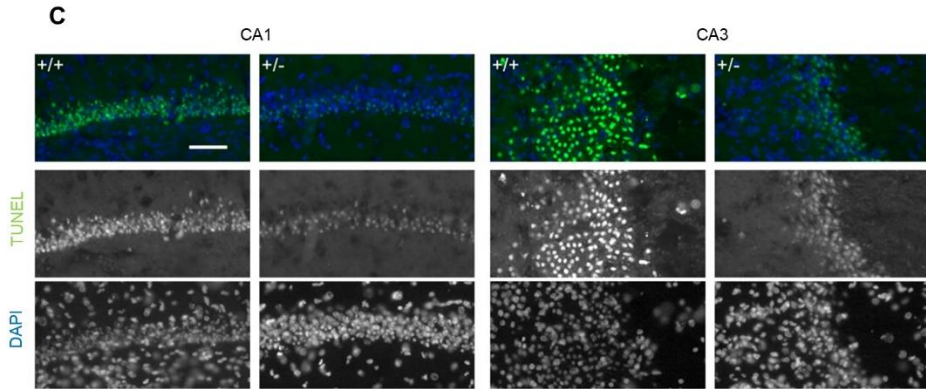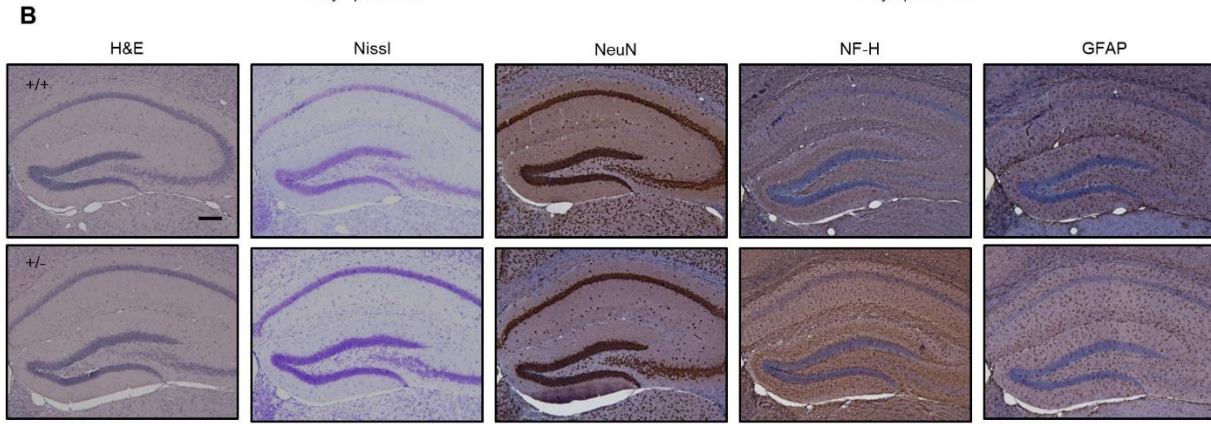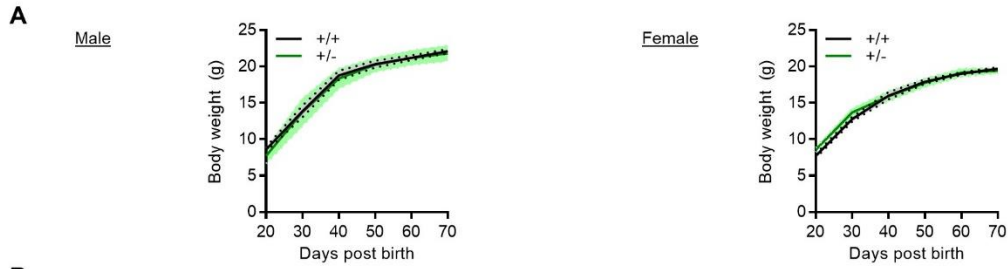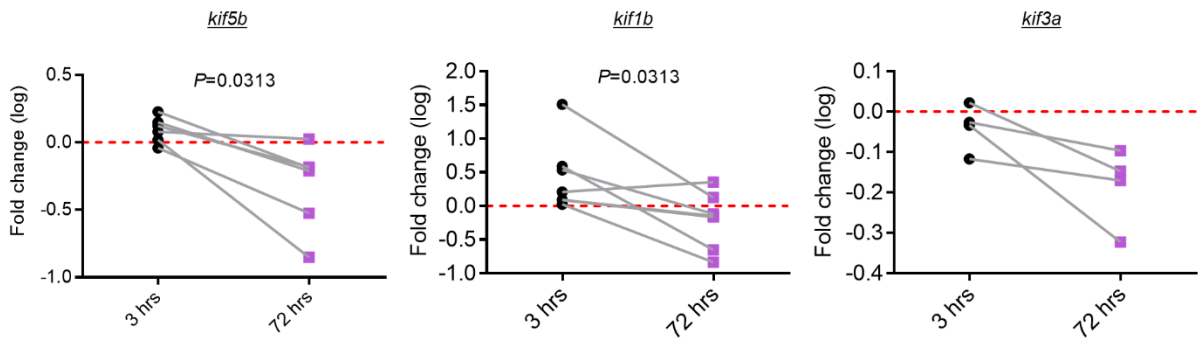**Figure S6 Reduced kif5b expression in the transcriptome of mouse cortex after ischemia preconditioning, related to Figure 6.**

(A) The expression profiling of kinesin genes (kifs) compared with the overall gene expression profile at 3 hrs (left) or 24 hrs (right) after IPC normalized to 72 hrs in the sham control. (B) Fold changes of *kif5b* (left), *kif1b* (middle) and *kif3a* (right) (Wilcoxon matched-pairs signed rank test).

Transparent Methods

Animals

The experimental protocol for this study was approved by the Committee on the Use of Live Animals in Teaching and Research, the University of Hong Kong. The target construct bearing a loxP site between exon 2 of the *kif5b* gene was electroporated into embryonic stem cells. Stable transfectants were selected and mice were generated according to standard protocols (Cui et al., 2011). Heterozygous mice were backcrossed with C57 mice for at least four generations for use in the study.

Cell culture and transfection

Primary neuronal cultures were prepared from P0 mice as previously described (Beaudoin et al., 2012), but with minor modification. Briefly, mouse forebrains were dissected under a dissection microscope by carefully removing the meninges but leaving the cortex and hippocampus intact. The tissues were digested using papain and seeded at a concentration of 0.5 to 2 x 10^6 cells per mL. After 48 hours, AraC (2 μM) was added to halt the proliferation of non-neuronal cells. A mixed culture of cortical and hippocampal neurons yielded more cells and were used in the excitotoxicity and calcium assays. A 293T cell line was maintained in Dulbecco's modified Eagle's medium (Invitrogen) with 10% fetal bovine serum (Gibco) and passaged every 2 days.

Transfection of primary neurons was performed within 3-5 days in vitro (DIV) for transfection of GFP-GluN2B in *kif5b*$^{+/-}$ neurons and their wild-type counterparts, or within 8-9 DIV for co-transfection of 3XFLAG-Kif5b/mutants and GFP-GluN2B in *kif5b*$^{+/-}$ neurons. Transfection of 293T cells was performed the next day after passage to 90% confluence. Lipofectamine 2000 (Invitrogen) was used to transfect DNA into cells. Briefly, 5 μL Lipofectamine and 3 μg DNA were added to the cultures in a 60-mm dish. After transfection for 6 hours, half of the medium in the neuronal culture was replaced to minimize cytotoxicity.

Antibodies, plasmids, and reagents

All chemicals were purchased from Sigma unless otherwise indicated. The antibodies used included rabbit polyclonal anti-actin, mouse monoclonal anti-α-tubulin, mouse monoclonal anti-GFAP, mouse monoclonal anti-PSD-95, mouse monoclonal anti-neurofilament heavy chain, rabbit polyclonal anti-KIF17, mouse monoclonal anti-FLAG, and rabbit polyclonal anti-FLAG antibodies (Sigma); mouse monoclonal anti-nNOS, goat polyclonal anit-KLC1, and goat polyclonal anti-GIPC antibodies (Santa Cruz); rabbit polyclonal anti-GluN1, rabbit polyclonal anti-GluN2A, rabbit polyclonal anti-GluN2B, and rabbit polyclonal anti-KLC antibodies (Millipore); rabbit polyclonal anti-KIF5a, rabbit polyclonal anti-Kif5b, and rabbit polyclonal anti-Kif5c antibodies (Abgent); monoclonal anti-KIF3 antibody (Covance); rabbit polyclonal anti-myc, and rabbit polyclonal anti-NeuN antibodies (Abcam); and mouse monoclonal anti-Munc-18, and mouse monoclonal anti-syntaxin-6 antibodies (BD Bioscience). Other antibodies used included normal rabbit, mouse and goat IgG (Santa Cruz); HRP-conjugated secondary antibodies for Western blotting (Invitrogen); FITC, Cy3, Cy5, and DyLight conjugated secondary antibodies for immunofluorescence (Jackson Immunoresearch); and Alexa-conjugated secondary antibodies (Invitrogen).

The complementary DNAs (cDNAs) encoding KIF5b truncations were generated by PCR and subcloned into pGEX4T1 or 3XFLAG-pcDNA3.1(+) vectors. The cDNA encoding GFP-GluN2B was kindly provided by Dr. J. H. Luo (University of Zhejiang, Hangzhou, China). The cDNA encoding GluN1-1a

was kindly provided by Dr. A. F. Stephenson (School of Pharmacy, University of London, London, UK). Deletion/truncation mutants and positively charged amino acids mutants were constructed by PCR and were verified by sequencing.

Excitotoxicity and cell death assessment

The primary neuronal cultures were exposed to the excitotoxin on 12-14 DIV. Briefly, cells were washed in control solution (CS) containing NaCl (121 mM), KCl (5 mM), D-glucose (20 mM), HEPES (17 mM), sodium pyruvate (1 mM), sodium bicarbonate (3 mM), and calcium chloride (1.8 mM). Cells were exposed to the indicated concentration of NMDA in CS, 6-cyano-7-nitroquinoxaline-2,3-dione (CNQX, 10 μM), and nimodipine (NIM, 10 μM) for 10 minutes. After NMDA was washed off, cells were incubated in CS without sodium pyruvate. After 24 hours, cell death was quantified by propidium iodide (PI) staining and by morphological analysis under a phase contrast microscope. In addition, LDH released into the medium was measured using a cytotoxicity detection kit (Roche) according to the manufacturer's instructions. For the negative control, neurons were incubated in CS with CNQX/NIM/MK801/NMDA/glycine. For the positive control ("all-kill"), neurons were incubated in CS with CNQX/NIM/NMDA/glycine overnight. Cells were exposed to kainate in CS with MK-801 (10 μM) and NIM (10 μM) in an incubator overnight. For the blockade assay, cells were incubated for 20 minutes in the experimental reagents prepared in CS before exposure to NMDA. The dead fraction was calculated by normalizing the LDH level of the treatment group to the "all-kill" group.

Cell death assessment in GFP-transfected neurons after excitotoxic insult

On 10 DIV, primary cortical and hippocampal neurons from $kif5b^{+/-}$ mice were transfected with GFP, GFP-2A-Kif5b^{FL}, GFP-2A-Kif5b$^{\Delta Ai}$ or GFP-2A-Kif5b$^{\Delta Ms}$ constructs by a calcium phosphate precipitation method (Clontech). After 24 hours, neurons were subject to excitotoxic insult in NMDA (50 μM) for 10 min, and the NMDA was then washed off. The control sister cultures were subjected to sham wash and incubation. After 24 hours post-treatment, images were taken using a Nikon Eclipse Ti-S/L100 inverted microscope using SPOT software 5.0. Healthy transfected neurons were quantified in each group. Cell death was identified by the presence of fluorescent cell debris and fragmented neurites. For each group, 800-1600 positive neurons were observed in four to six independent experiments. The fraction of dead cells was calculated as 1 minus the ratio of the number of healthy positive neurons in the treatment groups to the number in the control sister groups.

Biotinylation assay of surface-expressed receptors

Brain slices were obtained from adult $kif5b^{+/-}$ mice and their wild-type littermates (P42–P60) using previously described procedures (Tjong et al., 2008). Briefly, mice were anesthetized by methoxyflurane inhalation and then decapitated. The brains were quickly removed and chilled in ice-cold artificial cerebrospinal fluid (ACSF) in 95% O_2 / 5% CO_2. A tissue block containing the hippocampus was isolated and sectioned transversely into 400-μm thick slices using a vibroslicer. Slices were equilibrated in ACSF aerated with 2 mL/min 95% O_2 / 5% CO_2 at 36°C ± 1°C at least 30 minutes prior to the experiments. Humidified and warmed 95% O_2 / 5% CO_2 gas was continuously directed over the slices.

Samples were pre-cooled on ice to halt intracellular biological processes before biotinylation (Thomas-Crusells et al., 2003). For surface protein labeling, slices were washed twice with ice-cold phosphate-buffered saline (PBS) and incubated in ACSF containing 1.5 mg/mL NHS-SS-Biotin (Pierce) for 10

minutes at room temperature. Unreacted biotin was quenched and removed by two washes in ACSF containing 0.1 M glycine. Total soluble lysate was harvested by solubilizing the cells in RIPA buffer, and 20% of the volume was removed as the "lysate" sample. The remaining total lysate was incubated in Streptavidin resin (Pierce) overnight at 4°C with end-over-end shaking. The resin was subsequently removed by washing four times in solubilization buffer and eluted by boiling with loading buffer containing sodium dodecyl sulfate (SDS) and dithiothreitol. Samples were then subjected to SDS-polyacrylamide gel electrophoresis (PAGE) and Western blot analysis.

Co-immunoprecipitation and pull-down assays

The 293T cells, mouse cortex, or hippocampus were homogenized in buffer containing HEPES (20 mM), NaCl (150 mM), EDTA (2 mM), EGTA (2 mM), NP-40 (0.5%), and protease inhibitors (Roche). The cleared supernatants were incubated with the respective primary antibody or normal IgG raised from the same species as the negative control for 1 hour at 4°C. Protein-G or Protein-A agarose beads (Roche) were washed in Co-IP buffer and incubated with the antibody-bound lysate overnight at 4°C with up-and-down rotation. The bound agarose was collected by centrifugation and then washed three times using a Co-IP buffer. The samples were eluted using SDS-PAGE loading buffer and resolved by SDS-PAGE and subjected to immunoblotting.

Microtubule co-sedimentation

Mouse brain tissue was collected and homogenized in buffer containing PIPES (0.1 M, pH 6.8), EGTA (2 mM), and $MgSO_4$ (1 mM), and centrifuged at 1000 g for 10 minutes and then at 100,000 g for 30 minutes at 4°C. Taxol (40 μM) and GTP (1 mM) were added to the supernatant and incubated for 15 minutes at 37°C with gentle shaking. The supernatant was divided into two portions, one with ATP (2 mM) and one with AMP-PNP (2 mM), and then incubated for 30 minutes at 37°C. The supernatants were placed onto a 60% glycerol cushion and centrifuged at 100,000 g for 40 minutes at 20°C. Both supernatant and pellet were analyzed by Western blotting.

Immunofluorescence

For surface labeling, the antibodies were diluted in culture medium with HEPES (20 mM) and incubated with primary cells for 30 minutes at 4°C. Cells were fixed with freshly made 4% paraformaldehyde (PFA) and 4% sucrose in PBS for 10 minutes at room temperature, followed by permeabilization with 0.25% Triton X-100 in PBS for 5 minutes at room temperature. After blocking with 10% BSA/PBS, the cells were incubated with the primary antibody for either 2 hours at room temperature or overnight at 4°C. The cells were washed three times with PBS and incubated with the secondary antibody for 1 hour at room temperature. The cells were then washed with PBS three times and mounted on a glass slide in mounting medium (DAKO). The number of GluN2B positive puncta was counted manually and the GluN2B positive puncta intensity was measured in ImageJ.

Calcium imaging

Neurons cultured on poly-l-lysine-coated coverslips or in 12-well plates were labeled with 5 μM calcium indicator dye Fluo-3 AM (Invitrogen) in Neurobasal medium for 40 minutes at 37°C. NMDA stimulation was done at 14 D. I. V. or after, while KCl induced depolarization was done within 10 D. I. V.. The cells were washed and incubated in Neurobasal medium for 15 minutes prior to the analysis. Neurons were incubated in control solution at 37°C and imaged using a Perkin Elmer Spinning Disc Confocal

microscope (excitation, 488 nm; emission, 500–560 nm) with a continuous scan rate (512 × 512 pixels, 2 s per frame). Neurons were rested in control solution with CNQX (10 μM) and Nifedipine (Nif; 10 μM) prior to NMDAR stimulation. The cells were treated with NMDA (50 μM) and glycine (20 μM) to activate whole-cell NMDARs with continuous imaging after a 50-frame baseline scan.

The activation of synaptic and extrasynaptic NMDAR was performed as previously described (Tu et al., 2010). Synaptic NMDARs were activated by treatment with Bicuculline (Bic, 50 μM)/4-AP (2 mM). After reaching the peak response, MK-801 (10 μM, final concentration) was added to suppress synaptic NMDARs. The synaptic NMDAR signal was determined from the signal intensity before and after administration of MK-801. After washoff and resting in control solution with CNQX (10 μM) and Nif (10 μM), extrasynaptic NMDARs were activated by treatment with NMDA (50 μM) and glycine (20 μM) with continuous imaging. For depolarization, the neurons were rested in control solution and depolarized with 70 mM KCl in control solution. The data was analyzed by MetaMorph (Molecular Device) and presented as $\Delta F/F_0$, where F_0 is the average baseline fluorescence intensity and ΔF is the difference between baseline and the evoked fluorescence intensity.

NO emission assay

The NO emission from acutely prepared hippocampal slices was measured using an NO-sensitive electrode (Tjong et al., 2008). The tip of the NO electrode was gently placed at the CA1 stratum pyramidale on the hippocampal slice under visual guidance. The current was measured at a voltage of 0.85 V using a CHI 660A electrochemical analyzer (CH Instruments). The NO electrode was fabricated using a platinum wire insulated in a polyethylene tube dipped in Nafion. The Nafion-coated electrode was further modified with palladium and iridium oxide particles. The NO electrode was calibrated with successive injections of various concentrations of NO standards (20-1000 nM) into the perfusate in the recording chamber. The NO standards were prepared by serial dilution of phosphate-buffered saline saturated with NO gas (Matheson). The NO calibration plot was linear with a correlation coefficient ($y = a + bx$) not less than 0.95. The current response of the NO electrode was examined before and after the experiment and was calibrated using the NO standard curve.

Cerebral ischemia

Middle cerebral artery occlusion (MCAO) was performed in mice as previously described (Lo et al., 2005). Briefly, mice (male, 10-12 weeks) were anesthetized (induced with 2% halothane in a 70:30 mixture of nitrous oxide/oxygen, and maintained in 1% halothane in a 70:30 mixture of nitrous oxide/oxygen). To occlude the right middle cerebral artery at its origin, an 8-0 filament coated with vinyl polysiloxane (3M Dental Products, USA) was inserted into the right internal carotid artery. To ensure adequate occlusion and arterial reperfusion, continuous laser Doppler flowmetry (Perimed, Sweden) was applied to monitor the relative cerebral blood flow (CBF) in the right middle cerebral artery core territory via an attached optic fiber glued to the skull (2.0 mm posterior from bregma and 6.0 mm lateral from the sagittal suture). After filament insertion, anesthetic gas was continuously supplied for an additional 5 minutes to maintain the ischemia. After removing the anesthetic, mice were maintained in a temperature-controlled incubator (ThermoCare® intensive care unit system, ThermoCare Inc, USA) at 30°C. Mice were anesthetized again at 1 hour and 50 minutes after ischemia. At 2 hours after ischemia, the filament was removed to allow reperfusion. An additional 5 minutes of anesthesia was applied and the animal was kept in an incubator for an additional 4 hours. A heating pad was used to maintain the rectal temperature at about 37°C ± 1.5°C during the whole procedure.

Neurological deficits were evaluated at 24 hours after reperfusion. Briefly, mice were scored in a blinded manner based on the following index: 0, no observable neurological deficits (normal); 1, failure to extend opposite forepaw (mild); 2, circling to the contralateral side (moderate); and 3, loss of walking and righting reflex (severe). Mice were then sacrificed, and brains were sectioned into five 2-mm thick coronal slices and stained with 2% 2,3,5-triphenyltetrazolium chloride (TTC) at 37°C in the dark to detect the ischemic area. The posterior surface of each brain slice was photographed and analyzed by ImageJ to determine the infarct area and infarct volume, which were estimated using the indirect method as previously described (Lo et al., 2005).

For bilateral common carotid occlusion (BCCAO), mice were anaesthetized and a midline incision was made to expose the common carotid artery on both sides. Both common carotid arteries were occluded for 5 minutes for preconditioning or 20 minutes for neurodegeneration. The blood flow blockage was removed and the incisions were sutured using a 5-0 silk suture. The mice were returned to their cage with free access to food and water. Mice were sacrificed 2 days (preconditioning) or 7 days (neurodegeneration) after BCCAO by overdose with anesthetic, and brain tissue was collected for histology or immunoblotting.

Immunohistochemistry

Brain samples were fixed in 4% PFA/PBS and then immersed in 30% Sucrose/PBS overnight at 4°C. The samples were embedded in OCT medium (Leica) and sectioned into 25-µm thick slices using a Cryostat (Leica) and stored at -80°C. For histology and TUNEL assays, slices were dried thoroughly and rehydrated in 100% to 50% ethanol, followed by 2 minutes in ddH$_2$O. For immunohistochemistry, slices were air dried and rehydrated in PBS for 10 minutes.

Statistical analysis

The sample size was chosen according to standard practice in the field. Data distribution was assumed to be normal and was determined by Shapiro–Wilk test using SigmaStat 3.5. No randomization could be applied except in the experiments where mice or primary culture were divided into different treatment groups and genotypes. At least three independent experiments were performed for the statistical analysis. Data were expressed as mean ± s.e.m. in all figures, unless otherwise indicated, and 'n' denotes the total number of analyzed specimens. Student's unpaired t-test was used for comparisons between two groups (GraphPad Prism 6). One-way analysis of variance (ANOVA) with Sidak post hoc test was used for the analysis of more than two groups, and two-way ANOVA with Sidak post hoc test was used for the analysis of two different treatments between genotypes (GraphPad Prism 6). The exact methods and values are indicated in the text and figure legends. Signal intensities in the densitometric analysis of the Western blots were normalized to loading controls or total protein levels as indicated. P values less than 0.05 were considered significant.

Supplemental References

Beaudoin, G.M.J., Lee, S.-H., Singh, D., Yuan, Y., Ng, Y.-G., Reichardt, L.F., and Arikkath, J. (2012). Culturing pyramidal neurons from the early postnatal mouse hippocampus and cortex. Nat Protocols *7*, 1741-1754.

Cui, J., Wang, Z., Cheng, Q., Lin, R., Zhang, X.-M., Leung, P.S., Copeland, N.G., Jenkins, N.A., Yao, K.-M., and Huang, J.-D. (2011). Targeted Inactivation of Kinesin-1 in Pancreatic β-Cells In Vivo Leads to Insulin Secretory Deficiency. Diabetes *60*, 320-330.

Lo, A.C., Chen, A.Y., Hung, V.K., Yaw, L.P., Fung, M.K., Ho, M.C., Tsang, M.C., Chung, S.S., and Chung, S.K. (2005). Endothelin-1 Overexpression Leads to Further Water Accumulation and Brain Edema after Middle Cerebral Artery Occlusion via Aquaporin 4 Expression in Astrocytic End-Feet. Journal of Cerebral Blood Flow & Metabolism *25*, 998-1011.

Thomas-Crusells, J., Vieira, A., Saarma, M., and Rivera, C. (2003). A novel method for monitoring surface membrane trafficking on hippocampal acute slice preparation. Journal of Neuroscience Methods *125*, 159-166.

Tjong, Y.-W., Li, M., Hung, M.-W., Wang, K., and Fung, M.-L. (2008). Nitric oxide deficit in chronic intermittent hypoxia impairs large conductance calcium-activated potassium channel activity in rat hippocampal neurons. Free Radical Biology and Medicine *44*, 547-557.

Tu, W., Xu, X., Peng, L., Zhong, X., Zhang, W., Soundarapandian, M.M., Balel, C., Wang, M., Jia, N., Zhang, W.*, et al.* (2010). DAPK1 interaction with NMDA receptor NR2B subunits mediates brain damage in stroke. Cell *140*, 222-234.